XRD reflection-intensity ratios in slate slabs as detectors of incipient calcite fabric in slates

Autor(en): **Kisch, Hanan J.**

Objekttyp: **Article**

Zeitschrift: **Schweizerische mineralogische und petrographische Mitteilungen = Bulletin suisse de minéralogie et pétrographie**

Band (Jahr): **82 (2002)**

Heft 2: **Diagenesis and Low-Grade Metamorphism**

PDF erstellt am: **24.04.2024**

Persistenter Link: https://doi.org/10.5169/seals-62358

Nutzungsbedingungen

Die ETH-Bibliothek ist Anbieterin der digitalisierten Zeitschriften. Sie besitzt keine Urheberrechte an den Inhalten der Zeitschriften. Die Rechte liegen in der Regel bei den Herausgebern.
Die auf der Plattform e-periodica veröffentlichten Dokumente stehen für nicht-kommerzielle Zwecke in Lehre und Forschung sowie für die private Nutzung frei zur Verfügung. Einzelne Dateien oder Ausdrucke aus diesem Angebot können zusammen mit diesen Nutzungsbedingungen und den korrekten Herkunftsbezeichnungen weitergegeben werden.
Das Veröffentlichen von Bildern in Print- und Online-Publikationen ist nur mit vorheriger Genehmigung der Rechteinhaber erlaubt. Die systematische Speicherung von Teilen des elektronischen Angebots auf anderen Servern bedarf ebenfalls des schriftlichen Einverständnisses der Rechteinhaber.

Haftungsausschluss

Alle Angaben erfolgen ohne Gewähr für Vollständigkeit oder Richtigkeit. Es wird keine Haftung übernommen für Schäden durch die Verwendung von Informationen aus diesem Online-Angebot oder durch das Fehlen von Informationen. Dies gilt auch für Inhalte Dritter, die über dieses Angebot zugänglich sind.

Ein Dienst der *ETH-Bibliothek*
ETH Zürich, Rämistrasse 101, 8092 Zürich, Schweiz, www.library.ethz.ch

http://www.e-periodica.ch

SCHWEIZ. MINERAL. PETROGR. MITT. 82, 169–185, 2002

XRD reflection-intensity ratios in slate slabs as detectors of incipient calcite fabric in slates

by *Hanan J. Kisch*[1]

Abstract

Lattice preferred orientation (LPO) of calcite is difficult to measure in rocks rich in mica, since the "basal" *00·l* and "prismatic" *hk·0* X-ray reflections of calcite are weak or masked by mica reflections. The calcite reflections 01·8 at 47.5° and 20·2 at 43.2 °2Θ (CuKα radiation) correspond to a flat (*e*) and a steep (*M*) rhombohedron, their intensities are oppositely affected by LPO, and they do not coincide with strong reflections of other common phases. The departure of their intensity ratio, $IR_{47.5°/43.2°}$, in cleavage-parallel (C), bedding-parallel (B), and intersection-normal (⊥I) slabs from that in randomly oriented calcite can therefore be used as an approximate indicator of incipient calcite LPO in phyllosilicate-rich, fine-grained rocks, in which calcite fabric is hard to detect by other means.

Sixteen samples of Tertiary flysch with incipient cleavage from the Helvetic zone of the Swiss Alps were investigated. All show low $IR_{47.5°/43.2°}$ in the ⊥I slabs, indicating a calcite *c*-axis or *e*-pole LPO subnormal to I. High $IR_{47.5°/43.2°}$ in the C slabs of most of the samples indicate a large angle of this fabric to cleavage. Relatively high $IR_{47.5°/43.2°}$ in the B slabs in some of the samples reflect persistence of an earlier bedding-normal calcite *c*-axis/*e*-pole fabric, in many cases a bedding-parallel cleavage. In the case of small cleavage-bedding (C∠B) angles, these cases cannot be unequivocally distinguished, due to the convergence of the $IR_{47.5°/43.2°}$ in the C and B slabs. The method gives the best results at high C∠B angles; additional information on the orientation of the *c*-axis/*e*-pole LPO fabric is obtained from plots of $I_{47.5°}$* against $I_{43.2°}$* as normalized against $I_{48.6°}$ as a parameter of calcite content in the slabs.

Plots of $IR_{47.5°/43.2°\,C}$ / $IR_{47.5°/43.2°\,\perp I}$ vs. $IR_{47.5°/43.2°\,C}$ / $IR_{47.5°/43.2°\,B}$ can be used to assess the intensity of tectonic calcite-fabric development in samples with different C∠B angles and different pre-deformational bedding-normal calcite *c*-axis LPO fabrics; the $IR_{47.5°/43.2°}$ C/⊥I ratio is tentatively proposed as an indicator of this intensity. The calcite fabrics detected are much weaker than those of the phyllosilicates, suggesting that the phyllosilicates reorient largely by passive mechanical rotation through removal of matrix by pressure solution.

Keywords: Calcite fabric, lattice-preferred orientation (LPO), slate, incipient cleavage, X-ray diffraction methods, Helvetic flysch.

1. Introduction

The ratios of the basal and prismatic X-ray diffraction peaks obtained on mineral aggregates with a preferred *c*-axis lattice orientation (LPO) diverge from those in randomly oriented aggregates: they are higher in sections normal to, and lower in sections parallel to this fabric. This difference can be used to detect preferred mineral orientations in fine-grained rocks.

In an earlier study of the intensity ratios of the basal 10-Å and 7-Å XRD reflections in slate slabs cut parallel to cleavage and bedding as an estimate of the extent of phyllosilicate orientation (KISCH, 1998), an attempt was made to assess the calcite content of the samples from the intensity of the calcite 10·4 and 01·2 reflections at 29.4 °2Θ and 23.1 °2Θ (CuKα radiation). The intensity ratios of these reflections – $I_{29.4°}/I_{23.1°}$ – in the cleavage- and bedding-parallel slabs of the same specimens were found to show appreciable differences. Since these reflections correspond respectively to the slightly oblate positive cleavage rhombohedron $r\{10\bar{1}1\}$ at an angle of 44.61° to the base $c(0001)$, and the steeper negative rhombohedron f $\{02\bar{2}1\}$ at an angle of 63.12° to the base $c(0001)$, these differences in reflection-intensity reflect the development of a calcite LPO in the speci-

[1] Department of Geological and Environmental Sciences, Ben-Gurion University of the Negev, P.O. Box 653, Beer-Sheva 84 105, Israel. <kisch@bgumail.bgu.ac.il>

mens (the position of the various calcite forms mentioned are shown in stereographic projection on Fig. 1).

Calcite fabrics in deformed limestones of the Helvetic nappes show *c*-axis and *e* 01·8 maxima at high angles to the cleavage (cf. SCHMID et al., 1981; DIETRICH and SONG, 1994). A calcite fabric also develops in shales and siltstones during incipient stages of cleavage development (RAMSAY and HUBER, 1983, p. 179). However, such calcite fabrics are difficult to determine optically due to fine grain, and by X-ray methods due to low calcite content (weak reflections) and overlap of some X-ray diffraction peaks by those of accompanying phases, such as muscovite/phengite, precluding their use in mica-rich specimens. For this reason, an attempt is made here to detect calcite LPO's by use of the intensity ratios of reasonably strong near-basal and near-prismatic calcite X-ray reflections that are not compounded by reflections of other major phases in the rocks.

2. Choice of calcite reflections as LPO parameters

The most suitable parameters for the detection of *c*-axis LPO's are *hk·0* and *00·l* reflections corresponding to prismatic and basal forms. However, the "prismatic" reflection 03·0 at 64.7 °2Θ and the "basal" reflection 00·12 at 65.6 °2Θ are both weak, with $I/I_{1\ ASTM\ 5\text{-}0586} = 5$ and $= 3$, respectively (cf. DIETRICH, 1986, p. 656); the prismatic reflection 11·0 at 36.0 °2Θ, which has been used in X-ray texture analyses of calcite (e.g. DIETRICH and SONG, 1984), is reasonably strong ($I/I_{1\ ASTM\ 5\text{-}0586} = 14$), but cannot be used in mica-rich specimens since it almost coincides with the 008 reflection of $2M_1$ muscovite/phengite, the intensity of which is very different in the bedding- and cleavage parallel slabs of shales and slates with a strong muscovite or phengite fabric.

The interfacial angles of the slightly oblate cleavage rhombohedron $r\{10\bar{1}1\}$ at an angle of 44.61° to the base *c*(0001) and rr' $10\bar{1}1 \wedge \bar{1}101 = 74.92°$, and the steeper $f\{01\bar{1}2\}$ rhombohedron at an angle of 63.12° to the base *c*(0001) and ff' $02\bar{2}1 \wedge \bar{2}021 = 101.15°$, show a rather similar though opposite departure from 90°; the intensities of the corresponding 10·4 and 01·2 reflections at 29.4 °2Θ and 23.1 °2Θ might therefore be expected to be affected by *c*-axis fabrics in an opposite sense. Unfortunately, the 23.1 °2Θ reflection is compounded by the $1\bar{1}1$ albite and oligoclase reflections (with $I_{pk} = 11$–10), and attempts to correct for this overlap by reference to the intensity of the adjoining $\bar{2}01$ reflection of albite and oligoclase at 22.0 °2Θ did not give unequivocal results.

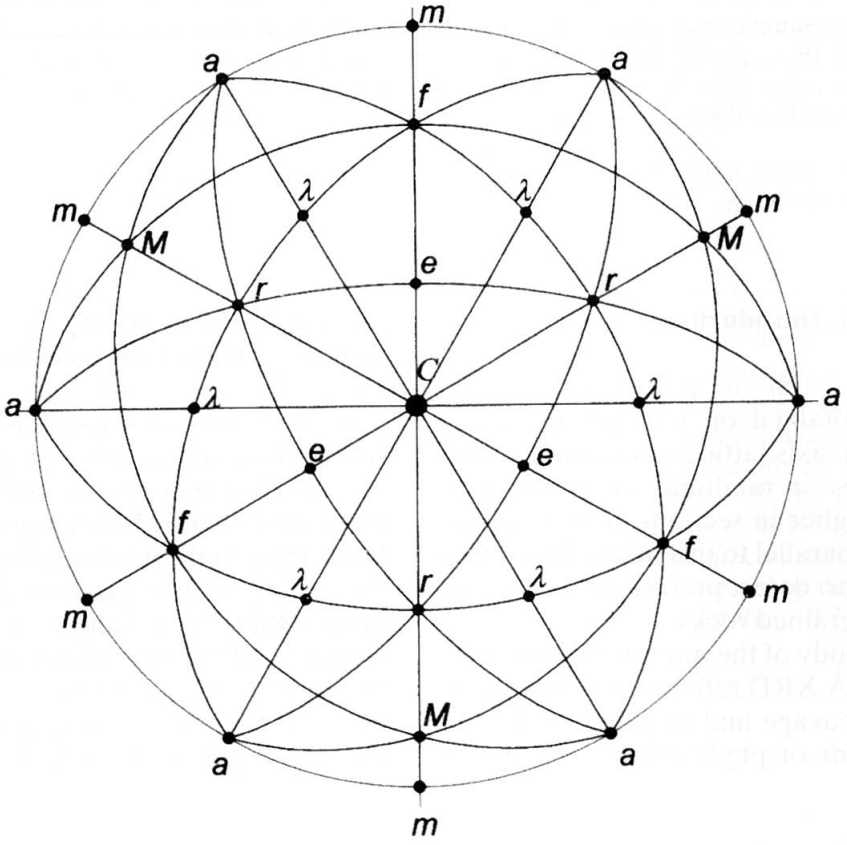

Fig. 1 Stereographic projection showing the faces of calcite discussed in the text; the angles between the various forms and the basal plane *c*(0001) are listed in Table 1.

For this reason, the *c*-axis LPO fabric effects are characterized here by use of the intensity ratios of reflections corresponding to a steep and an oblate rhombohedron, that are not compounded or compounded only to a very minor extent by reflections of other major phases in the rocks. Such two reflections are the *M* 20·2 reflection at 43.2 °2Θ ($I/I_{1\ ASTM\ 5\text{-}0586} = 18$) and the *e* 01·8 reflection at 47.5 °2Θ ($I/I_{1\ ASTM\ 5\text{-}0586} = 17$). These correspond respectively to the very steep positive rhombohedron *M* {40$\bar{4}$1} at an angle of 75.77° to (0001) and an interfacial angle *MM'* 40$\bar{4}$1 ^ $\bar{4}$401 = 114.17° and to the flat negative rhombohedron *e*{01$\bar{1}$2} at an angle of 26.25° to (0001) and an interfacial angle *ee'* 01$\bar{1}$2 ^ $\bar{1}$012 = 45.05°; the latter is also the plane of the ubiquitous lamellar *e* twinning of calcite. Since *e* and *M* are respectively negative and positive rhombohedra, for every *e* plane parallel to a slab, an *M* plane is oriented at ca. 102° to it. These reflections do not coincide with strong reflections of accompanying phases: the peak at 47.5 °2Θ is overlapped by the relatively minor $\bar{4}$22 peak($I_{pk} = 5$) of oligoclase An_{29} at 47.38 °2Θ (COLVILLE and RIBBE, 1966, 1968), but resolved from the analogous low-albite $\bar{4}$22 peak at 48.01 °2Θ and muscovite/phengite peaks. Since the plagioclase in slates is almost invariably pure albite, no attempt has been made to correct the intensity of the 47.5 °2Θ peak for the presence of oligoclase. However, when the method is applied to amphibolite or higher-grade facies rocks, a check should be made for the possible overlap of the 47.5 ° 2Θ peak by plagioclase reflections. The intensity ratio $I_{47.5°}/I_{43.2°}$, hence $IR_{47.5°/43.2°}$, is therefore adopted here as a parameter of calcite fabric.

It should be emphasized that, since the 01·8 peak used in lieu of a "basal" *00·l* peak and the 20·2 peak used in lieu of a "prismatic" *hk·0* peak correspond respectively to lattice planes *e*{01$\bar{1}$2} at an angle of 26.26° to (0001) and to lattice planes *M* {40$\bar{4}$1} at an angle of 75.77° to (0001), what is really being measured is the maximum or the minimum due to the *e*{01$\bar{1}$2} LPO fabric subparallel to or subperpendicular to the slabs. The use of these X-ray reflections precludes distinction between calcite *c*-axis and *e*{01$\bar{1}$2} pole LPO's, both of which have been reported. However, since in *c*-axis fabrics the poles on *e*{01$\bar{1}$2} form a small circle at 26° about the *c*-axis maximum, and, statistically there is little difference between the maxima of the *e*{01$\bar{1}$2} poles and the *c* axis (compare, e.g., TROMMSDORFF, 1964, Fig. 1, diagrams D1, D2 and D5, and Fig. 2, diagrams D7 and D9; SCHMID et al., 1981, Fig. 1, *c* and *e* patterns), there should be little difference between *e*{01$\bar{1}$2}-pole and *c*-axis maxima as measured on slabs.

Ideally, the intensity of only one orientation parameter, either the 20·2 reflection at 43.2 °2Θ or the 01·8 reflection at 47.5 °2Θ, normalized to the calcite content of the slab, could be used as an orientation parameter. However, normalization of peak intensities against the chemically determined carbonate content is difficult to carry out in practice for two reasons:

(a) The inhomogeneity of the samples due to lithologic bedding, particularly in the slabs cut at an angle to the bedding, since the slabs cut from a sample in different directions may have significantly different calcite contents, as evident from plots of peak intensity and peak-sum intensity of

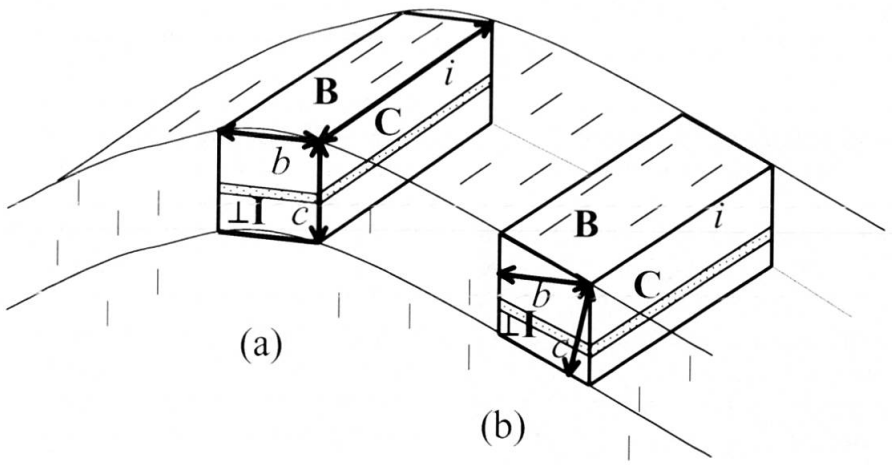

Fig. 2 Schematic sketch showing the position of the cleavage-parallel (C), bedding-parallel (B) and intersection-normal (⊥I) slabs, as well as the direction of the fissility-fragment dimension parameters *c*, *b* and *i* discussed in sections 6.4 to 6.6. (a) Bedding and cleavage orthogonal; (b) bedding and cleavage non-orthogonal. Note that *c*, *b*, and *i* are the normal spacings of bedding, cleavage and transverse cracks, respectively, but at orthogonal or nearly orthogonal bedding and cleavage *c*, *b*, and *i* may be measured as fragment lengths and width parallel to the 'cleavage', 'bedding' and 'intersection' directions, respectively.

the calcite peaks measured on slabs cut parallel to cleavage and to bedding (hence referred to as C and B slabs; see Fig. 2) against the carbonate content as determined by weight loss; such plots show appreciable scatter for the intensities and intensity combinations from slabs cut from the same sample in different directions.

(b) The variable dolomite content of the samples, which is apparent from the low values of peak intensity and peak-sum intensity of the calcite peaks for given carbonate contents as determined by weight loss, and in some samples from appearance of a distinct 30.95 °2Θ diffraction peak in the diffractograms.

Conceivable X-ray diffraction parameters of calcite content in a slab are the intensities of either a calcite reflection that is not or only to a very minor extent affected by differences in calcite fabric, or, alternatively, a combination of two calcite reflections that are similarly but oppositely affected by differences in calcite fabric. Such peak intensities include those of the 10·4 reflection at 29.4 °2Θ (hence $I_{29.4\,°2\Theta}$) which corresponds to the cleavage rhombohedron $r\{10\bar{1}1\}$ and the 11·6 reflection at 48.6 °2Θ (hence $I_{48.6\,°2\Theta}$), which corresponds to the second-order pyramid $\lambda\{22\bar{4}2\}$, a form with twelve rather than six faces. Since the contribution of the lattice planes corresponding to each of these twelve faces to the total reflection intensity is relatively small, the reflection intensities of such many-faced forms are less likely to be affected by accidental orientation of a face parallel to the slab.

A possible combination of peak intensities is the geometric mean of the 43.2 °2Θ and 47.5 °2Θ peaks (hence $\sqrt{(I_{43.2\,°2\Theta} * I_{47.5\,°2\Theta})}$.

The intensities of these potential indicators of calcite content in slabs are compared in the results section.

3. Effects of calcite LPO on the $IR_{47.5°/43.2°}$ intensity ratios of slabs

Presence of a calcite *c*-axis/$e\{01\bar{1}2\}$-pole LPO enhances the intensity of basal reflections ($I_{00\cdot l}$) and flat-rhombohedral reflections (such as $I_{01\cdot 8}$) and suppresses that of prismatic reflections ($I_{hk\cdot 0}$) and acute-rhombohedral reflections (such as $I_{20\cdot 2}$) in slabs cut perpendicular to that fabric. This increases the intensity ratio $I_{subbasal}/I_{subprismatic}$ (hence $IR_{sbs/spr}$) in the slabs cut perpendicular to this fabric above the value for randomly oriented calcite, and lowers it in the slabs cut perpendicular to it.

In the following, the intensity ratios $IR_{sbs/spr}$ measured on slabs are plotted normal to those slabs. Thus plotted, the intensity-distribution of a (sub)basal or flat-rhombohedral reflection measured on the slabs represents a section of the orientation-density distribution of the pole on such reflections, the crystallographic *c*-axis or the pole on $e\{01\bar{1}2\}$.

3.1. ORIENTATION-DENSITY DRIBUTION OF THE CALCITE *c*-AXES AND *e*-POLES

The pole figures of low-temperature calcite tectonites from the Helvetic Alps (SCHMID et al., 1981, Fig. 1; WENK, 1985, Fig. 18a, c; RUTTER et al., 1994, Fig. 1), and three specimens deformed in the twinning regime at shear strains (γ) of 1.1–1.2 (SCHMID et al., 1987, Fig. 10a–d) show distinct *c*-axis and pole to $e\{01\bar{1}2\}$ maxima. Admittedly, many calcite fabrics have a preferred orientation in rotation about the *c* axis , but commonly this is expressed by a single maximum in the *a*-axis girdle normal to the *c*-axis maximum (e.g. SCHMID et al., 1981, Fig. 1; WENK, 1985, Fig. 18b, d; RUTTER et al., 1994, Fig. 1), which does support the approximate similarity of the shape of the polar orientation distribution of $IR_{47.5°/43.2°}$ to a triaxial ellipsoid with long axis near the *c*-axis/*e*-pole maximum and short axis near the *a*-axis maximum.

Strictly, the polar orientation density distribution will be roughly ellipsoidal only if the deformation is homogeneous. If the deformation becomes partitioned and inhomogeneous on the scale of the slabs, by local oriented crystallization of new calcite crystals – for instance along the cleavage domains –, this calcite orientation will be superimposed on the primary bedding fabric in the microlithons. The orientation-density distribution in the plane normal to the cleavage/bedding intersection then should acquire a bimodal, incomplete girdle or "butterfly" shape formed by superimposition of an ellipse with long semiaxis parallel to the new *c*-axis/*e*-pole LPO upon an ellipse with its long semiaxis normal to the bedding – in case of persistence of an earlier bedding-subnormal *c*-axis or *e*-pole LPO in the microlithons of a crenulation cleavage. Such transitional "incomplete girdle patterns with orthorhombic or monoclinic symmetry" of muscovite and chlorite (002) poles have been interpreted by SINTUBIN (1994, Figs. 5 and 8 and pp. 228–229) as showing "the development of a secondary spaced cleavage on a primary, continuous, bedding-parallel cleavage". In the following we assume that deformation is homogeneous on the scale of the sample.

Table 1 Calcite forms and the corresponding X-ray reflections referred to in the text, with difraction angles, relative peak intensities ($I_{29.4°} = 100$) measured on powdered calcite front-packed and side-packed in sample holders, on three perpendicular slabs of two Senonian chalks from Tel Beer-Sheva and an Eocene chalk from Bet-Guvrin, southern Israel, and on powdered chalks from Bet-Guvrin and Tel Beer-Sheva.

	hkil	Angle	*hk·l*	2Θ	I/I_1	Diffraction-peak intensities								
	cl. rhomb.	with	X-ray	(CuK_α)	ASTM	calcite powder			means of three chalk slabs			chalk powders	
	cell	*c*(0001)	cell		5-0586	(a)	(b)	(c)	(d)	(e)	(f)	(g)	(h)	(i)
f	$02\bar{2}1$	63.12°	01·2	23.1°	12	6.6	6.0	8.8	10.48	9.76	9.37	9.87	8.98	8.06
r	$10\bar{1}1$	44.61°	10·4	29.4°	100	100	100	100	100	100	100	100	100	100
a	$11\bar{2}0$	90°	11·0	36.0°	14	7.8	7.8	10.3	13.31	12.47	12.64	12.81	11.92	10.13
α	$44\bar{8}3$	66.30°	11·3	39.4°	18	n.m.	11.4	16.0	18.61	18.05	17.60	18.09	17.43	16.13
M	$40\bar{4}1$	75.77°	20·2	43.2°	18	9.7	10.6	13.6	15.79	15.01	14.78	15.20	14.79	13.10
e	$01\bar{1}2$	26.26°	01·8	47.5°	17	15.2	15.6	14.7	16.93	16.65	16.86	16.81	18.80	16.06
λ	$22\bar{4}3$	48.72°	11·6	48.6°	17	13.2	13.8	15.5	18.05	17.49	17.19	17.57	17.84	16.39
m		90°	03·0	64.7°	5	3.1	3.2	5.58	4.89	5.04	4.81	4.91	4.73	4.06
c		0°	00·12	65.6°	3	2.9	2.7	2.40	2.51	2.64	2.88	2.68	2.90	2.77

Diffraction-peak intensities: (a) front packed; (b) front packed, ½° divergence/scatter slits; (c) side-packed.
(d), (e) and (f) are the geometric means of the intensities of one bedding-parallel and two bedding-normal slabs of chalks (d) TS-1 (Senonian), (e) TS-3 (Senonian), and (f) BG-01 (Eocene); (g) mean of (d), (e) and (f); (h) and (i) front packed powdered chalk powders of chalks (h) BG-01 and TS-3.
All measurements except (b) with 1° divergence/scatter slits. Intensities are peak-heights in percentages of the 29.4° 2Θ peak height.

3.2. ORTHOGONAL SLABS PARALLEL AND PERPENDICULAR TO AN ELLIPSOIDAL CALCITE LPO

For an ellipsoidal polar orientation distribution, if cleavage is normal to bedding, and a polar LPO is normal to one of three mutually perpendicular slabs, and one ellipsoid axis is parallel to the cleavage/bedding intersection I – i.e., the other two respectively are normal to cleavage and bedding –, the orientation of the ellipsoid is entirely known, and *the three ratios measured suffice to unequivocally define the shape of the ellipsoid.* Since the geometric mean $\sqrt[3]{(r_1 \cdot r_2 \cdot r_3)}$ of the three orthogonal coordinate semiaxes r_1, r_2 and r_3 of an ellipsoid equals the radius R of a sphere with similar volume, this should then apply to the peak-intensity ratios of the polar plots of the $IR_{sbs/spr}$ ratios $IR_{sbs/spr\ r1}$, $IR_{sbs/spr\ r2}$, and $IR_{b/p\ r3}$ on three perpendicular slabs cut parallel to the principal sections of the ellipsoid: their geometric mean, $\sqrt[3]{(IR_{sbs/spr\ r1} \cdot IR_{sbs/spr\ r2} \cdot IR_{sbs/spr\ r3})}$, should equal the radius of a sphere representing the peak-intensity ratio in randomly oriented calcite, hence $IR_{sbs/spr\ R}$.

$IR_{sbs/spr\ r3}$ on the slab r_3 normal to the polar LPO maximum should be *higher* than this random value $IR_{sbs/spr\ R}$, and in both the two perpendicular slabs r_1 and r_2 *lower* than $IR_{sbs/spr\ R}$ *by a smaller amount*; the geometric mean of the two latter, $\sqrt{(IR_{sbs/spr\ r1} \cdot IR_{sbs/spr\ r2})}$, should equal $\sqrt{(IR_{sbs/spr\ R}^3/IR_{sbs/spr\ r3})} - IR_{sbs/spr\ r1}$ equaling $IR_{sbs/spr\ r2}$ if the polar distribution is a uniaxial prolate ellipsoid subnormal to slab r_3.

A low $IR_{sbs/spr}$ in a slab indicates an enhanced *c*-axis or *e*-pole fabric (hence: polar fabric) along its surface, but *not* its orientation relative to the two perpendicular slabs: thus, it could reflect a polar fabric (1) normal to bedding, (2) normal to cleavage, or even (3) a random distribution around I. In all three cases the geometric mean of $IR_{sbs/spr\ C}$ and $IR_{sbs/spr\ B}$ should approximately equal $\sqrt{(IR_{sbs/spr\ R}^3/IR_{sbs/spr\ \perp I})}$. They may be distinguished by considering the relationship between $IR_{sbs/spr}$ in the B and C slabs: in cases (1) and (2) $IR_{sbs/spr}$ will be high in respectively the B and C slabs, and similarly low in both perpendicular slabs, as the latter are parallel to the preferred *c*-axis lineation; in case (3), $IR_{sbs/spr}$ in the C and B slabs should *both* be higher than in the ⊥I slab.

The above is valid only for an ellipsoidal polar-orientation distribution. In contrast, a bimodal butterfly-shaped polar-orientation distribution, with maxima normal to both the C and B slabs, should produce a value of $\sqrt{(IR_{sbs/spr\ C} \cdot IR_{sbs/spr\ B})}$ notably larger than $\sqrt{(IR_{sbs/spr\ R}^3/IR_{sbs/spr\ \perp I})}$.

3.3. SLABS OBLIQUE TO THE CALCITE LPO

Strictly, the above relationships hold only when the polar LPO maximum is normal to one of three mutually perpendicular slabs, i.e., not when it is *oblique* to one or more of the slabs.

In the case of orthogonal C and B slabs oblique to the calcite fabric, low $IR_{sbs/spr}$ in the ⊥I slab could also reflect a polar LPO maximum in a plane ⊥I but at an angle to both C and B. In this case, intermediate between (1) and (2), $IR_{sbs/spr}$ in the C and B slabs still should *both* be higher than in the ⊥I slab, but converge – becoming equal to each other when the fabric maximum bisects the angle between C and B. Moreover, $\sqrt{(IR_{sbs/spr\ r1} \cdot IR_{sbs/spr\ r2})}$ is somewhat smaller than $\sqrt{(IR_{sbs/spr\ R3}/IR_{sbs/spr\ r3})}$, this reduction being at a maximum when the polar LPO maximum bisects the angle between the slabs, and increasing with the eccentricity of the $IR_{sbs/spr\ r1}$, $IR_{sbs/spr\ r2}$ ellipse in the ⊥I plane: for a 45° angle it is 0.95 for an eccentricity of 1.5, and 0.90 for an eccentricity of 2.0, a value rarely reached in the investigated samples.

Although $IR_{47.5°/43.2°}$ is only an approximation to the $IR_{sbs/spr}$, formation of calcite crystals with a *c*-axis fabric should increase $IR_{47.5°/43.2°}$ in the slabs cut normal to that fabric above its value for randomly oriented calcite, 1.1 (cf. Table 1, column g), and lower it in the slabs cut parallel to that fabric.

The ⊥I -slab is always cut perpendicular to the C and B slabs, but the angle between C and B in many of the samples is much smaller, as small as 25°. Even when the orientation distribution of the *c* axes or *e* poles is ellipsoidal, the product of the $IR_{sbs/spr}$ or $IR_{47.5°/43.2°}$ ratios on such two non-orthogonal C and B slabs may be higher or lower than the product of the ratios on two orthogonal slabs, depending on whether the fabric maximum lies in the obtuse or the acute angle between these non-orthogonal slabs, and therefore cannot be expected to indicate in a simple manner whether the polar-orientation distribution is ellipsoidal or not.

4. Methods

Diffraction traces were run on cleavage-parallel, bedding-parallel and intersection-normal slabs (hence: C slab, B slab and ⊥I slab) of 16 Helvetic flysch slates used in the earlier study (for lithology and localities see KISCH, 1998, Table 1), with CuKα radiation, using fixed 1° divergence and scatter slits and a 0.2 mm receiving slit, at counting rates of not less than 10^3. The slabs were scanned from 19° to 66 °2Θ. The calcite reflections

Table 2 Peak heights of X-ray reflections at 29.4°, 43.2°, 47.5° and 48.6°2Θ in slabs, and C∠B angles.

	C slab				B slab				⊥ I slab				C∠B
Sample nr	$I_{29.4°}$	$I_{43.2°}$	$I_{47.5°}$	$I_{48.6°}$	$I_{29.4°}$	$I_{43.2°}$	$I_{47.5°}$	$I_{48.6°}$	$I_{29.4°}$	$I_{43.2°}$	$I_{47.5°}$	$I_{48.6°}$	
Z91-2A	1490	236	328	322	2290	280	367	354	1384	242	167	228	25
Z91-3	660	–	–	–	614	–	–	–	636	–	–	–	75
Z91-3 2° slits	–	368	453	436	–	348	348	396	–	360	350	418	75
Z91-4	1096	190	219	207	1130	156	184	176	920	178	166	176	45
Z91-7	3250	380	696	566	2160	432	288	362	2700	480	382	480	75
Z91-9	2164	304	348	422	2460	400	410	446	1440	292	294	304	20
Z91-11	803	–	–	–	778	–	–	–	528	–	–	–	40
Z91-11 2° slits	–	330	468	450	–	442	504	508	–	444	380	452	40
Z91-12A	706	160	140	193	860	152	174	103	544	108	100	76	20
Z91-12A 2° slits	–	92	120	127	–	136	130	94	–	104	116	68	20
Z91-13	1860	280	320	374	2190	300	386	372	1610	292	298	300	25
Z91-20	110	–	–	–	94	–	–	–	748	124	110	120	40
Z91-21	996	–	–	–	602	–	–	–	872	–	–	–	90
Z91-21 2° slits	–	266	435	395	–	362	272	316	–	618	482	578	90
Z91-22	2730	444	547	528	1760	260	300	346	–	–	–	–	
Z91-23	2980	404	412	423	3360	464	492	546	3308	496	488	524	35
Z91-25	3240	576	498	568	3760	536	544	556	3990	620	576	636	60
Z91-26	3360	380	600	480	3860	520	656	594	3420	596	482	574	25
Z91-29A	246	–	–	–	894	–	–	–	694	–	–	–	40
Z91-29A 2° slits	–	128	158	146		456	384	416	–	496	343	400	40
Z91-31	2520	396	468	448	2556	360	386	415	2776	408	368	446	60
Calcite	16160	1574	2458	2130	–	–	–	–	5340	830	908	958	–
Calcite ½° slits	6100	650	951	839	–	–	–	–	–	–	–	–	–
Chalk	–	–	–	–	2244	384	372	406	2204	350	364	412	–

All values are peak heights in c.p.s Measurements with 1° divergence and scatter slits unless otherwise indicated.

measured are listed in Table 1, with the relative peak intensities ($I_{29.4°}$ = 100) measured on powdered calcite front-packed and side-packed in sample holders, and on bedding-normal and bedding-parallel slabs of a Senonian chalk from Tel Beer-Sheva. Peak-height intensities were hand-measured on the diffraction traces. On slabs with peak-height intensities of less than 100 c.p.s. (25 mm on the diffraction trace) of one or more of the reflections at 43.2, 47.5 and 48.6 °2Θ, these three reflections were re-measured with fixed 2° divergence and scatter slits. Using a divergence slit of 2°, the X-ray beam will completely cover a 2 cm long sample at 2Θ angles larger than 37.1°; however, since 2Θ of the three reflections measured differ very little, even incomplete interception of the X-ray beam by smaller or mis-positioned slabs will reduce the ratio of the intensity of the reflection at 43.2° to that at 48.6° at most by a factor of 0.9 [= sin (43.2°/2)/sin(48.6°/2)].

Even the powdered calcite showed some orientation effects as apparent from differences in relative intensities between the front- and side-packed powders. The almost consistently lower relative intensities from the front-packed samples (except for the basal 65.6° reflection, and only a very minor difference in the 47.5° reflection) indicate enhancement of the 29.4° reflection, presumably by pressing the powder in the sample holder.

5. Results

5.1. CALCITE PEAK-INTENSITY RATIOS IN THE C, B AND ⊥I SLABS

The calcite-peak intensities measured in the three slabs of each specimen are listed in Table 2, and the peak-intensity ratios in Table 3.

$IR_{47.5°/43.2°}$ for the three slabs of each sample are plotted on Fig. 3 against the carbonate content as estimated by the mean intensity of the 48.6 °2Θ reflection. Carbonate content was also determined by weight loss and TGA (thermogravimetric analysis), but these weight losses do not necessarily reflect calcite content, which is indicated by the intensities of the reflections at 48.6° and 29.4 °2Θ to be much lower in some of the samples. Sample 12A contains major dolomite and only subordinate calcite (mainly in veins), sample 11 also has an appreciable dolomite content, and samples 3 and 21 have notable siderite contents. Calcite in sample 12A occurs mainly in coarse veins, which results in inconsistent results upon use of different divergence/scatter slit sets, this sample is therefore ignored in the following discussion.

The results show marked difference in fabric between the samples, but there are some basic similarities between the patterns of the relation-

Table 3 X-ray reflection intensity ratios $I_{47.5°}/I_{43.2°}$, $I_{47.5°}/I_{48.6°}$, $I_{43.2°}/I_{48.6°}$, $\sqrt{(I_{43.2°}*I_{47.5°})}/I_{48.6°}$ and C∠B angles.

	$I_{47.5°}/I_{43.2°}$ ($IR_{47.5°/43.2°}$)			$1.16/\sqrt{(I_{47.5°}/I_{43.2°} \perp I\ 1°)}$	$I_{47.5°}/I_{48.6°}$			$I_{43.2°}/I_{48.6°}$			$\sqrt{(I_{43.2°}*I_{47.5°})}/I_{48.6°}$			C∠B
Slab nr	C	B	⊥I 1°		C	B	⊥I 1°	C	B	⊥I 1°	C	B	⊥I 1°	
Z91-2A	1.39	1.31	0.690	1.40	1.02	1.04	0.732	0.733	0.791	1.06	0.864	0.906	0.882	25
Z91-3 2° slits	1.23	1.00	0.972	1.18	1.04	0.879	0.837	0.844	0.879	0.861	0.936	0.879	0.849	75
Z91-4	1.15	1.18	0.933	1.20	1.06	1.05	0.943	0.918	0.886	1.01	0.985	0.963	0.977	45
Z91-7	1.83	0.667	0.796	1.30	1.23	0.796	0.796	0.671	1.19	1.00	0.909	0.974	0.892	75
Z91-9	1.14	1.02	1.01	1.16	0.825	0.919	0.967	0.720	0.897	0.961	0.771	0.908	0.964	20
Z91-11 2° slits	1.42	1.14	0.856	1.26	1.04	0.992	0.841	0.733	0.870	0.982	0.873	0.929	0.909	40
Z91-12A	0.875	1.14	0.926	1.21	0.725	1.69	1.32	0.829	1.48	1.42	0.775	1.58	1.37	20
Z91-12A 2° slits	1.30	0.956	1.12	1.10	0.945	1.38	1.71	0.724	1.45	1.53	0.827	1.41	1.62	20
Z91-13	1.14	1.29	1.02	1.15	0.855	1.04	0.993	0.748	0.806	0.973	0.799	0.915	0.983	25
Z91-20	–	–	0.887	1.23	–	–	0.917	–	–	1.03	–	–	0.973	40
Z91-21 2° slits	1.64	0.751	0.780	1.32	1.10	0.861	0.834	0.673	1.15	1.07	0.861	0.993	0.944	90
Z91-22	1.23	1.15	–	–	1.04	0.867	–	0.841	0.751	–	0.933	0.807	–	
Z91-23	1.02	1.06	0.984	1.17	0.974	0.901	0.931	0.955	0.850	0.947	0.964	0.875	0.939	35
Z91-25	0.865	1.01	0.929	1.21	0.877	0.978	0.906	1.01	0.964	0.975	0.943	0.971	0.940	60
Z91-26	1.58	1.26	0.809	1.29	1.25	1.10	0.840	0.792	0.875	1.04	0.995	0.983	0.934	25
Z91-29A 2° slits	1.23	0.842	0.692	1.40	1.08	0.923	0.858	0.877	1.10	1.24	0.974	1.01	1.03	40
Z91-31	1.18	1.07	0.902	1.22	1.04	0.930	0.825	0.884	0.867	0.915	0.961	0.898	0.869	60
Calcite 1°	1.56	–	1.09	1.11	1.15	–	0.947	0.739	–	0.866	0.924	–	0.906	–
Calcite ½°	1.46	–	–	–	1.13	–	–	0.775	–	–	0.937	–	–	–
Chalk 1°	–	0.969	1.04	1.05	–	0.916	0.883	–	0.946	0.850	–	0.931	0.866	–

Intensity ratios are based on measurements with 1° divergence/scatter slits unless otherwise indicated.

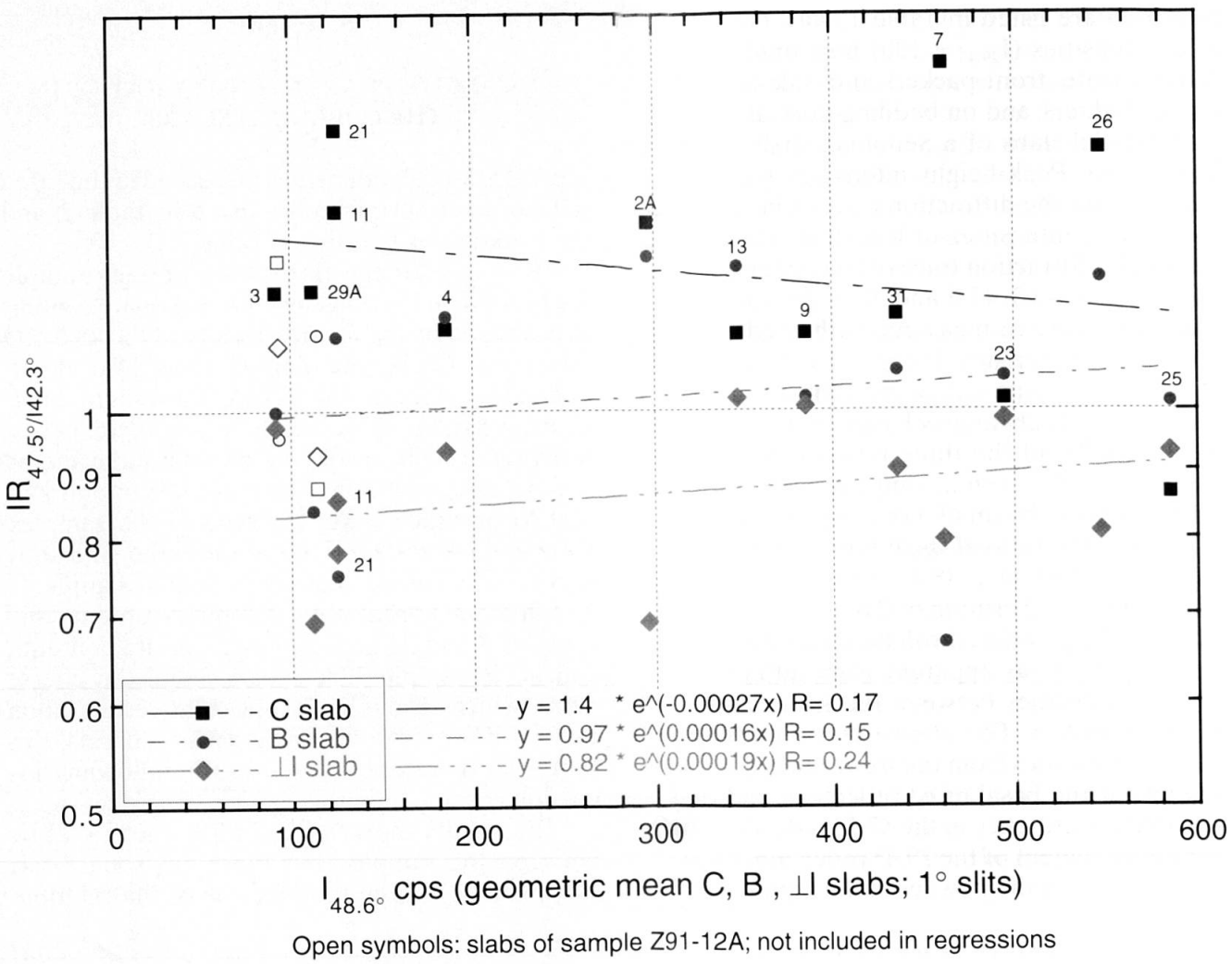

Fig. 3 Lack of variation of the fabric parameter $IR_{47.5°/43.2°}$ in the three slabs of each sample with calcite content as estimated by the geometric mean of the intensities of the reflection at 48.6 °2Θ in the three slabs. Note that the mean $I_{48.6°}$ values are based exclusively on measurements using 1° divergence/scatter slits, even for samples for which the $IR_{47.5°/43.2°}$ ratio is based on measurements with 2° slits.

ship of $IR_{47.5°/43.2°}$ of the three slabs: in the ⊥I slabs of all the samples $IR_{47.5°/43.2°}$ is 0.69–1.02, well below the value in random calcite, ca. 1.05, and appreciably lower than in either the C or B slabs (3 samples) or commonly than in both (10 samples), indicating a *c*-axis/*e*-pole LPO maximum subnormal to I. $IR_{47.5°/43.2°}$ in the C slabs ranges from 0.86 to 1.83; in the B slabs from 0.67 to 1.3.

In three of the most calcite-rich samples [22, 23, 25], $IR_{47.5°/43.2°}$ of the three slabs show little difference: they vary between 0.86 and 1.2 – indicating little calcite fabric.

The relationships between $IR_{47.5°/43.2°}$ in the three slabs appear to represent three basically different relationships:

1. Appreciably lower $IR_{47.5°/43.2°}$ in the ⊥I slabs than in both the C and B slabs, which are similarly high, suggesting a strong *c*-axis/*e*-pole LPO at a high angle to both the C and B planes, i.e. in their obtuse angle: samples Z91-2A, 4, both with small C∠B angles and crenulation cleavage, cf. KISCH, 1998, Table 1); probably 22.

2. Appreciably lower $IR_{47.5°/43.2°}$ in both the ⊥I and C slabs than in the B slab, indicating a strong *c*-axis/*e*-pole fabric subnormal to I and subparallel to C: sample Z91-12A (1° slits), with small B∠C angle.

Transitional relationship #1–2: $IR_{47.5°/43.2°}$ low in ⊥I, intermediate in C, and high in B slab, indicating a *c*-axis/*e*-pole fabric at a higher angle to B than to C: sample Z91-13.

These calcite fabrics with a fabric maximum at a high angle to the bedding are either pre-existent, probably reflecting the persistence of bedding-parallel cleavage fabric detected earlier in some of these samples (KISCH, 1998, p. 603), or due to coarse-grained vein calcite (Z91-12A).

3. Appreciably lower $IR_{47.5°/43.2°}$ in both the B and ⊥I slabs than in the C slab, indicating strong *c*-axis/*e*-pole fabric subnormal to I and subparallel to B (and subnormal to C, when the angle C∠B is close to 90°): samples Z91-3, 7, 21, all with large

C∠B angles of 75–90°. Similarly low $IR_{47.5°/43.2°}$ on the B and ⊥I slabs, as in samples 3 and 21, must indicate a prolate "cigar"-shaped *c*-axis or *e*-pole fabric subnormal to C.

Transitional relationship #1–3: $IR_{47.5°/43.2°}$ low in ⊥I, intermediate in B, and high in C slab, indicating a *c*-axis/*e*-pole fabric subnormal to I, but at a higher angle to C than to B: samples Z91-11, 26, 29A, 31 (C∠B angles of 25–60°).

In samples Z91-9, 23 and 25 the differences between $IR_{47.5°/43.2°}$ of the slabs are too small to attach much importance to.

It was earlier argued that for an ellipsoidal fabric-orientation distribution, $\sqrt{(IR_{sbs/spr\ C} \cdot IR_{sbs/spr\ B})}$, the geometric mean of $IR_{sbs/spr\ C}$ and $IR_{sbs/spr\ B}$ as measured on orthogonal C and B slabs, should equal $\sqrt{(IR_{sbs/spr\ C} \cdot IR_{sbs/spr\ B})_{calc}} = \sqrt{(IR_{sbs/spr\ R}{}^3/IR_{sbs/spr\ \perp I})}$. Therefore, $\sqrt{(IR_{47.5°/43.2°\ C} \cdot IR_{47.5°/43.2°\ B})}$ as measured on orthogonal C and B slabs should be close to $\sqrt{(IR_{47.5°/43.2°\ C} \cdot IR_{47.5°/43.2°\ B})_{calc}}$, where $\sqrt{(IR_{47.5°/43.2°\ C} \cdot IR_{47.5°/43.2°\ B})_{calc}}$ equals

$\sqrt{(IR_{47.5°/43.2°\ R}{}^3/IR_{47.5°/43.2°\ \perp I})} = \sqrt{(1.05^3/IR_{47.5°/43.2°\ \perp I})} = 1.08/\sqrt{(IR_{47.5°/43.2°\ \perp I})}$.

In all samples with C∠B ≥ 75°, nos. 3, 7, and 21, and in sample 31 with C∠B = 60° this is indeed found to be the case, which confirms the assumption of an approximately elliptical shape of the fabric orientation distribution in the section ⊥I rather than a bimodal rounded butterfly shape for which the geometric mean of $IR_{47.5°/43.2°}$ in the C and B slabs should be markedly higher than $\sqrt{(IR_{47.5°/43.2°\ C} \cdot IR_{47.5°/43.2°\ B})_{calc}}$. However, in samples with small C∠B angles, for which the geometric mean of the $IR_{47.5°/43.2°}$ ratios in the C and B slabs are very different from $\sqrt{(IR_{47.5°/43.2°\ C} \cdot IR_{47.5°/43.2°\ B})_{calc}}$, the interpretation of a bimodal, "rounded oblique cross" density distribution cannot be disproved.

5. 2. X-RAY DIFFRACTION PARAMETERS OF CALCITE CONTENT

The possible calcite-content parameters, intensities $I_{29.4\ °2\Theta}$ and $I_{48.6\ °2\Theta}$ were plotted against the mean intensity $\sqrt{(I_{43.2\ °2\Theta} * I_{47.5\ °2\Theta})}$ for the three slabs of each of 14 Helvetic slates (Fig. 4). Good regressions with respectively R = 0.983 ($I_{29.4\ °2\Theta}$) and R = 0.978 ($I_{48.6\ °2\Theta}$) are obtained, suggesting that the mean peak intensity $\sqrt{(I_{43.2\ °2\Theta} * I_{47.5\ °2\Theta})}$ and the intensities $I_{29.4\ °2\Theta}$ and $I_{48.6\ °2\Theta}$ are both unaffected or similarly affected by orientation effects. However, the points for $I_{48.6\ °2\Theta}$ show less scatter than those for $I_{29.4\ °2\Theta}$, and the regression

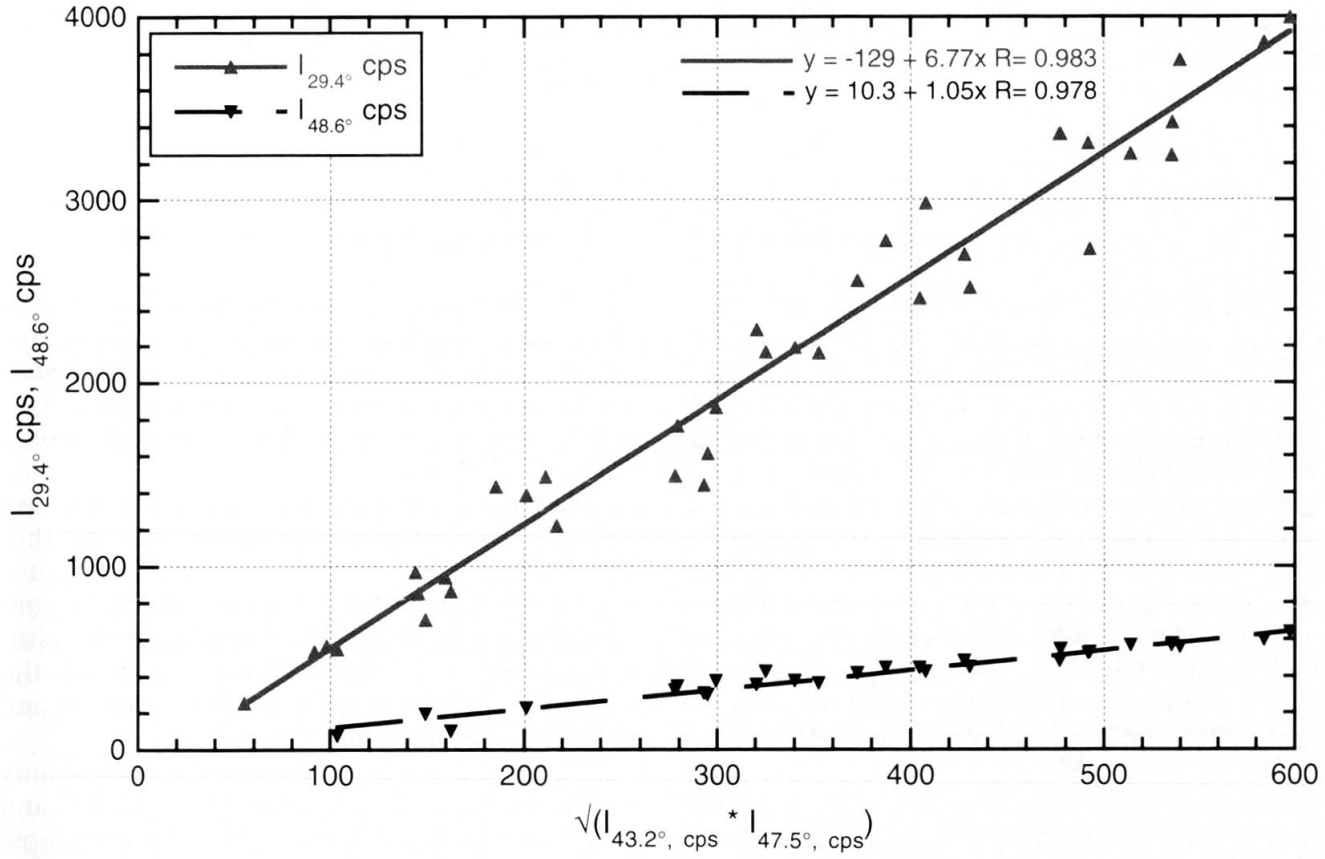

Fig. 4 Relationship between possible calcite-content parameters : variation of $I_{29.4°}$ and $I_{48.6°}$ with $\sqrt{(I_{43.2°} * I_{47.5°})}$. No calcite powder or chalk included. Considering the small y-axis intercept of the regression, the correlation of $I_{48.6°}$ with $\sqrt{(I_{43.2°} * I_{47.5°})}$ is much better than that of $I_{29.4°}$.

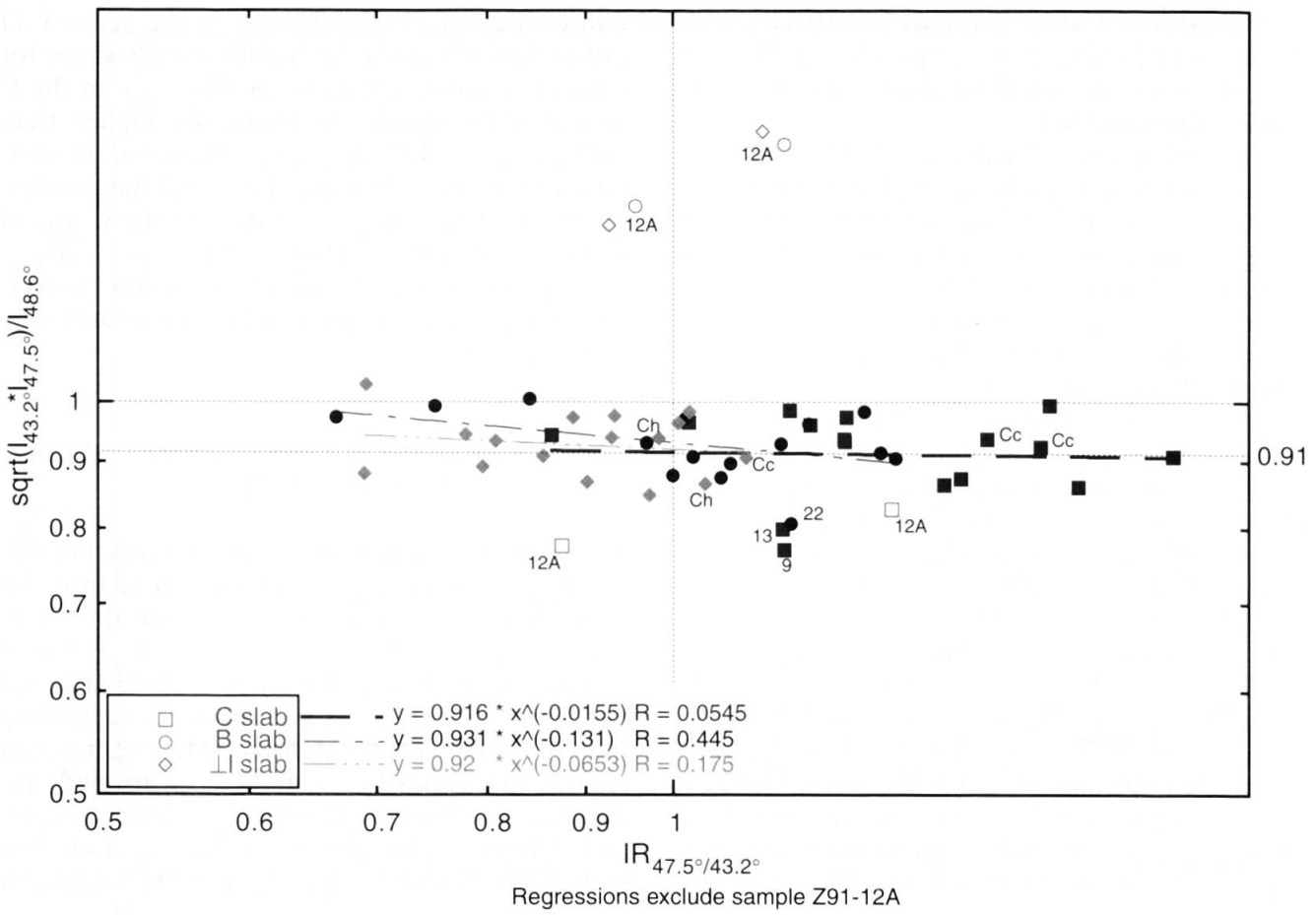

Fig. 5 Lack of dependence of the ratio of the calcite-content parameters $\sqrt{(I_{43.2^\circ} * I_{47.5^\circ})}/I_{48.6^\circ}$ ratio on the fabric parameter $IR_{47.5^\circ/43.2^\circ}$ for the C, B, and ⊥I slabs. Divergent slabs discussed in the text, calcite powders (Cc) and two chalk slabs (Ch) are labeled. Thin horizontal line indicates value of $I_{48.6^\circ}/\sqrt{(I_{43.2^\circ} * I_{47.5^\circ})}$ for randomly oriented calcite, 0.91 (data from Table 1, column g).

for $I_{48.6\,^\circ 2\Theta}$ passes appreciably closer to the origin than that for $I_{29.4\,^\circ 2\Theta}$, and therefore gives a much better fit.

This fit is confirmed by a plot of the $\sqrt{(I_{43.2\,^\circ 2\Theta} * I_{47.5\,^\circ 2\Theta})}/I_{48.6\,^\circ 2\Theta}$ ratio against the fabric parameter $IR_{47.5^\circ/43.2\,^\circ 2\Theta}$ (Fig. 5): the $\sqrt{(I_{43.2^\circ 2\Theta} * I_{47.5\,^\circ 2\Theta})}/I_{48.6\,^\circ 2\Theta}$ ratio remains relatively constant at 0.86 to 1.0 for a range of values of $IR_{47.5^\circ/43.2\,^\circ 2\Theta}$ from 0.67 to 1.83 – the value of $\sqrt{(I_{43.2\,^\circ 2\Theta} * I_{47.5\,^\circ 2\Theta})}/I_{48.6\,^\circ 2\Theta}$ for random calcite being 0.91. Two anomalous low $\sqrt{(I_{43.2\,^\circ 2\Theta} * I_{47.5\,^\circ 2\Theta})}/I_{48.6\,^\circ 2\Theta}$ ratios in the C slabs of Z91-9 and Z91-13 are considered to reflect very oblique angles between the *c*-axis/*e*-pole fabrics and these slabs, which cause low $\sqrt{(I_{43.2\,^\circ 2\Theta} * I_{47.5\,^\circ 2\Theta})}$, and possibly high $I_{48.6\,^\circ 2\Theta}$ that may appear when the *c*-axis fabric is at an angle of 41.3° to a slab, so that $\{22\bar{4}3\}$ becomes parallel to it. The $\sqrt{(I_{43.2\,^\circ 2\Theta} * I_{47.5\,^\circ 2\Theta})}/I_{29.4\,^\circ 2\Theta}$ ratio (not shown) is somewhat less constant: with increasing $IR_{47.5^\circ/43.2\,^\circ 2\Theta}$, it tends to decrease in the C and B slabs and increase in the ⊥I slab.

Tentatively, $I_{48.6\,^\circ 2\Theta}$ is adopted as an approximate parameter of calcite content.

5.3. RELATIONS BETWEEN THE $I_{48.6^\circ}$-NORMALIZED $I_{47.5^\circ}$* AND $I_{43.2^\circ}$* INTENSITIES

The low $IR_{47.5^\circ/43.2^\circ}$ ratios in the ⊥I slabs in most of the samples are due both to a lower $I_{47.5^\circ}$ reflecting development or reorientation of calcite crystals with *c* axes/*e* poles normal to I, and a higher $I_{43.2^\circ}$ due to suppression of calcite crystals with *c* axes/*e* poles parallel to I.

In order to assess to what extent the different $IR_{47.5^\circ/43.2^\circ}$ ratios reflect absolute changes in either $I_{43.2^\circ}$ or $I_{47.5^\circ}$, these were each normalized against $I_{48.6^\circ}$ as an approximate parameter of calcite content – hence $I_{43.2^\circ}$* and $I_{47.5^\circ}$* (see Table 3) –, plotted against each other and compared with the normalized ratios in random calcite powders and the chalk standard (Fig. 6).

The values of $I_{43.2^\circ}$* and $I_{47.5^\circ}$* for randomly oriented calcite are respectively around 0.87 and 0.96 (from Table 1, column g). The ⊥I slabs of most of the samples (2A, 4, 7, 11, 21, 26, 29A), show lower $I_{47.5^\circ}$* and higher $I_{43.2^\circ}$*. In the samples with small C∠B angles between 25° and 45°, these are

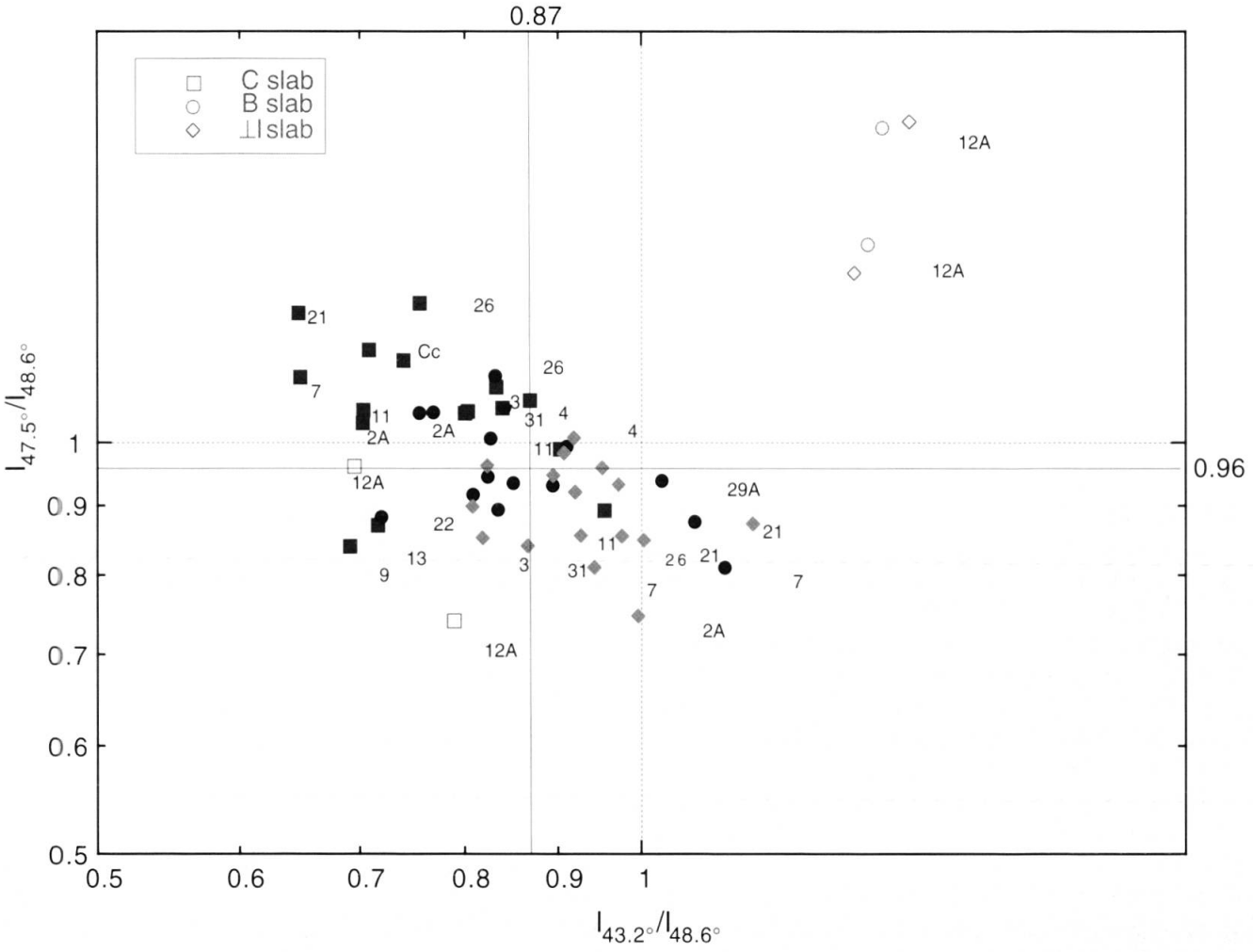

Fig. 6 Relationship of $I_{43.2°}$ and $I_{47.5°}$ as normalized against $I_{48.6°}$ for the C, B, and ⊥I slabs. Divergent slabs discussed in the text and two front-packed calcite powders (Cc) are labeled. Thin lines indicate values of $I_{43.2°}$* and $I_{47.5°}$* for randomly oriented calcite, 0.87 and 0.96 (data from Table 1, column g).

balanced by opposite values of *both* $I_{47.5°}$* and higher $I_{43.2°}$*, either equally in the C and B slabs (2A, 4), or predominantly in the C slab, and to a much lesser extent in the B slab (11, 26, 29A), indicating fabrics at similarly high angles to C and B or an appreciably higher angle to C than to B. Only in the samples with large C∠B angles of ≥ 75°, 7 and 21 (both belonging to group 3 of section 5.1), the balancing is entirely by the C slabs, which show the lowest $I_{43.2°}$* in the C slab of all samples, whereas the $I_{43.2°}$* in the B slabs is even higher than in the ⊥I slabs, indicating a fabric subparallel to both and subnormal to C, a combination of characteristics attainable only in samples with large C∠B angles.

Anomalously low values of *both* $I_{47.5°}$* and $I_{43.2°}$* are considered to reflect fabrics very oblique to those slabs. In two samples (3, 31), both with C∠B angles of ≥ 60°, such low values of both $I_{47.5°}$* and $I_{43.2°}$* in the ⊥I and B slabs are balanced mainly by the high $I_{47.5°}$* value of the C slabs, while the $I_{43.2°}$* values differ very little; the even lower values of both $I_{47.5°}$* and $I_{43.2°}$* in the C slabs of two samples (9, 13), with small C∠B angles of 20–25°, are possibly slightly exacerbated by anomalously high $I_{48.6°}$ values that could appear when the *c*-axis fabric is at an angle of 41.3° to a slab, so that $\lambda\{22\bar{4}3\}$ becomes parallel to it.

For the carbonate-rich slates with little difference between $IR_{47.5°/43.2°}$ in the three slabs [23, 25], there is little difference between the normalized $I_{43.2°}$* and $_{47.5°}$* intensities for the three slabs, all of which range between 0.85 and 1, the value for essentially random calcite fabrics.

The $I_{47.5°}$* versus $I_{43.2°}$* plot thus provides information on the orientation of the polar LPO fabrics in addition to that given by $RI_{47.5°/43.2°}$. If further study will show the effect of very oblique LPO fabrics on $I_{48.6°}$* to be negligible, $I_{47.5°}$* and $I_{43.2°}$* could be adopted as the main calcite LPO fabric parameters.

6. Discussion

6.1. CALCITE *c*-AXIS LPO IN DEFORMED LIMESTONES

In calcite rocks deformed at low temperatures, there is commonly a *c*-axis maximum normal to the foliation or at a small circle at 26° to the normal, and a great circle girdle of *a* axes in or at 26° to the foliation plane.

Axial compression at low temperatures of ≈200 °C (WENK et al., 1973; CASEY et al., 1978), and simple shear at 400–600 °C (FRIEDMAN and HIGGS, 1981) produce *c*-axis maxima parallel to the axis of greatest finite shortening, often with a second maximum at *e*{01·8}; this fabric is ascribed to twinning on *e*{01·8} (WENK, 1985). At higher temperatures (≈400 °C), the poles to *e*{01·8} shift to become parallel to the coaxial compression axis (WENK et al., 1973; WENK, 1985, Fig. 10c); experiments of coaxial and non-coaxial deformation of calcite rocks at 400 °C (RUTTER and RUSBRIDGE, 1977) produce *c* axes located at a small circle at 26° to σ_1. The *c*-axis maxima in many published pole figures of naturally deformed calcite rocks are slightly asymmetric, with angles of 25–45° to the normal to the foliation (WENK, 1985, Fig. 18).

SCHMID et al. (1981) found that the *c*-axis maxima in some limestones from unfolded sectors of the Helvetic nappes in western Switzerland were displaced from the foliation normal by 30° to 40°, in a sense opposite to the sense of shear. DIETRICH and SONG (1984) found that these *c*-axis maxima are subperpendicular to the XY plane or flattening plane defined by the grain-shape fabric indicated by the observed long axes of the grains; they ascribed the obliquity of this fabric to the macroscopic cleavage to the strain associated with a second-phase deformational event (cf. DIETRICH, 1986).

LT simple-shear pole figures show the same broad maximum as the pure-shear equivalents (where "the *c*-axes are concentrated in a broad maximum parallel to the main compression direction"), but its orientation is rotated against the sense of shear by up to 36° (WENK et al., 1987; SCHMID et al., 1987; DE BRESSER, 1989).

This obliquity with respect to the shear-plane normal has been used as a shear-sense indicator (e.g. SCHMID et al., 1987; DE BRESSER, 1989) and to determine the strain-path partitioning in calcite mylonites (RATSCHBACHER et al., 1991), but this use has been criticized by LAFRANCE et al. (1994).

The present results cannot distinguish between *c*-axis and *e*{01·8} maxima, but show that such maxima at high angles to the cleavage can be detected in incipient slates and siltstones at very low degrees of deformation, and are not restricted to pure calcite rocks

In the intracrystalline slip regime, at higher temperatures (500–700 °C) and/or lower strain rates, a *c*-axis maximum forms along a great circle roughly parallel to the flattening plane in addition to two *c*-axis maxima at high angles to the flattening plane (SCHMID et al., 1987, Fig. 14a, b and 15a), whereas in the even higher temperature (700–900 °C) grain-boundary sliding regime, the high-angle maxima disappear, and the maximum spreads along the great circle subparallel to the flattening plane (ibid., Fig. 18). The method proposed would detect such a maximum through the presence of high $IR_{47.5°/43.2°}$ in the C and ⊥I slabs. However, for such multiple *c*-axis maxima, the polar orientation of the *c*-axis distribution would be far from ellipsoid-shaped.

6.2. DEVELOPMENT OF CALCITE *c*-AXIS LPO UPON CLEAVAGE FORMATION: EFFECTS ON THE $I_{47.5}/I_{43.2°}$ RATIOS IN THE B AND ⊥I SLABS

A mudstone with a random calcite fabric has identical $IR_{47.5°/43.2°}$ for the three slabs. During RAMSAY and HUBER's (1983, Vol. 1, pp. 186–188) "cleavage stage of fabric development", the platy and acicular minerals are oriented in the cleavage plane, but generally without any linear alignment in the cleavage, since the total strain ellipsoid is now close to that of a uniaxial pancake. As preferential calcite *c*-axis orientation normal to cleavage develops during cleavage development as a result of flattening on C only, such a mudstone will develop an prolate *c*-axis fabric expressed by higher $IR_{47.5°/43.2°}$ in the C slabs than in both the B and ⊥I slabs. Upon flattening on C, the ratio in the C slab should increase at the expense of the "random" initial ratios of both the B slab and ⊥I slab.

In contrast, many rocks have a pre-existing bedding- normal calcite *c*-axis LPO fabric, either due to diagenetic compaction (cf. RAMSAY and HUBER, 1983, Vol. 1, p. 185; PATERSON et al., 1995) or to an earlier bedding-parallel cleavage. Such a fabric would be indicated by an initially high $IR_{47.5°/43.2°}$ in the B slab, and concomitantly low ratios in the ⊥I slab (and at high C∠B angles also in the C slab). Upon flattening on C, the initially low ratio in this slab should increase at the expense of *both* the high initial ratio in the B slab (at high C∠B angles) and the already low initial ratio in the ⊥I slab, whereas upon rotation of the calcite fabric around I (or simple shear normal to I), the ratio in

the C slab should increase mainly at the expense of the high initial ratio in the B slab, and to a much lesser extent of that in the ⊥I slab.

Only in the last stages of cleavage development – RAMSAY and HUBER's (1983, Vol. 1, p. 188) stage of "strong cleavage with stretching-lineation" –, the *c*-axis fabric may be accompanied by development of a stretch linear fabric on the cleavage surface of slates parallel to the tectonic X direction, subperpendicular to I, generally "down-dip", i.e. inclined to the fold axes at an angle approaching 90°. This lineation is partially defined by elongate minerals and mineral aggregates (e.g. HOBBS et al., 1976, p. 273). If accompanied by formation of calcite fibers with the *c*-axis parallel to the fiber length (DURNEY and RAMSAY, 1973), such extension would be evidenced by a concomitant decrease of the $IR_{47.5°/43.2°}$ ratio in the ⊥I slab, and reversal of its increase in the C slab and decrease in the B slab.

6.3. THE C∠B ANGLE AND DECREASE OF $IR_{47.5°/43.2°\ B}$ AND $IR_{47.5°/43.2°\ \perp I}$ UPON LPO DEVELOPMENT IN ROCKS WITH INITIALLY RANDOM FABRIC

We have seen that differences in the extent of compensation of the increase in $IR_{47.5°/43.2°}$ of the C slab with increasing *c*-axis/*e*-pole LPO can largely be explained in terms of differences in the C∠B angle. Let us assume a rock with an initially random calcite fabric, and flattening on C as the cleavage-forming mechanism. If the C and B slabs are normal to each other, any increase in $IR_{47.5°/43.2°}$ in the C slab will be accompanied by smaller but *similar* reductions in $IR_{47.5°/43.2°}$ in the B and ⊥I slabs. $IR_{47.5°/43.2°}$ in the B and ⊥I slabs will therefore remain equal throughout cleavage development, and their ratio $IR_{47.5°/43.2°\ B}$ / $IR_{47.5°/43.2°\ \perp I}$ (hence $IR_{47.5°/43.2°}$ B/⊥I), will remain at unity. When plotted on a ($IR_{47.5°/43.2°\ C}$ / $IR_{47.5°/43.2°\ \perp I}$) vs. ($IR_{47.5°/43.2°\ C}$ / $IR_{47.5°/43.2°\ B}$) plot – hence $IR_{47.5°/43.2°}$ C/⊥I vs. $IR_{47.5°/43.2°}$ C/B plot (Fig. 7)–, the points representing the same initial lithology and random calcite fabric should then constitute an approximately $IR_{47.5°/43.2°}$ B/⊥I-constant band at $IR_{47.5°/43.2°}$ B/⊥I = 1. In fact, the points representing samples with large C∠B angles (C∠B ≥ 60°) are distributed along a band with a slightly decreasing $IR_{47.5°/43.2°}$ B/⊥I with increasing $IR_{47.5°/43.2°}$ C/B (Fig. 7). We will address this point below.

As the C∠B angle decreases, the reduction in $IR_{47.5°/43.2°}$ of the ⊥I slab upon formation of a *c*-axis or *e*-pole fabric normal to C remains similar, whereas in the B slab is becomes progressively less, i.e., the $IR_{47.5°/43.2°}$ B/⊥I ratio now increases with progressive cleavage LPO formation. As the C∠B angle approaches 45°, increase in $IR_{47.5°/43.2°}$ in the C slab has equal effects on the $I_{47.5°}$ and $_{43.2°}$ in the B slab, and $IR_{47.5°/43.2°}$ in this slab is therefore unaffected by changes in this ratio in the C slab. At smaller C∠B angles, the points should then be distributed along bands that show increasing $IR_{47.5°/43.2°}$ B/⊥I ratios at higher $IR_{47.5°/43.2°}$ in the C slab, i.e. with a steeper $IR_{47.5°/43.2°}$ B/⊥I slope. This is shown on Fig. 7 by the regression for the samples with C∠B = 35–50°.

As the C∠B angle further decreases below 45°, increases in $IR_{47.5°/43.2°}$ in the C slab should actually result in smaller, but progressively larger *increases* in this ratio in the B slab, the theoretical end-member of this process being at C ‖ B (C∠B = 0°), when the increases in $IR_{47.5°/43.2°}$ in the B slab become identical to those in the C slab, and $IR_{47.5°/43.2°}$ C/B remains constant upon increasing C-parallel fabric.

In contrast to the $IR_{47.5°/43.2°}$ B/⊥I ratio, the increase in the $IR_{47.5°/43.2°}$ C/⊥I ratio during fabric development would *not* be affected by differences in the C∠B angle. The intensity ratio $IR_{47.5°/43.2°}$ C/⊥I would thus constitute a C∠B-independent fabric-development index.

6.4. INITIAL ANISOTROPY AND DEFORMATION INDEX AFTER DURNEY AND KISCH (1994)

DURNEY and KISCH (1994) made use of the fissility-fragment dimensions *c* and *b* – measured as fragment widths normal to the intersection direction in the cleavage and bedding, respectively (see DURNEY and KISCH, 1994, Fig. 3; this paper, Fig. 2) – to develop a relative cleavage/bedding fissility scale, and proposed use of the length of the fissility fragments in the direction of the cleavage/bedding intersection (*i*) to indicate the extent of tectonic fabric development in rocks with different initial bedding anisotropy. This method is based on the assumption that before deformation the intersection/bedding fissility ratio *i/b* was at unity, while the initial cleavage bedding fissility ratio c_0/b_0 at *i/b* = 1 represented the initial bedding/parallel anisotropy c_0/b_0. When plotted on a 3-axis logarithmic diagram, the distribution of the cleavage/bedding (*c/b*) and intersection/bedding (*i/b*) fissility ratios of slates with similar initial lithology are confined an I-constant band parallel to the *c/b* axis is obtained; the value of *c/b* at the intersection of the projected mean trend of this distribution with the *i/b* = 1 axis constitutes the c_0/b_0 ratio of the rock before deformation. The intersection/bedding fissility *i/b* is relatively independent of the initial bedding anisotropy, and therefore con-

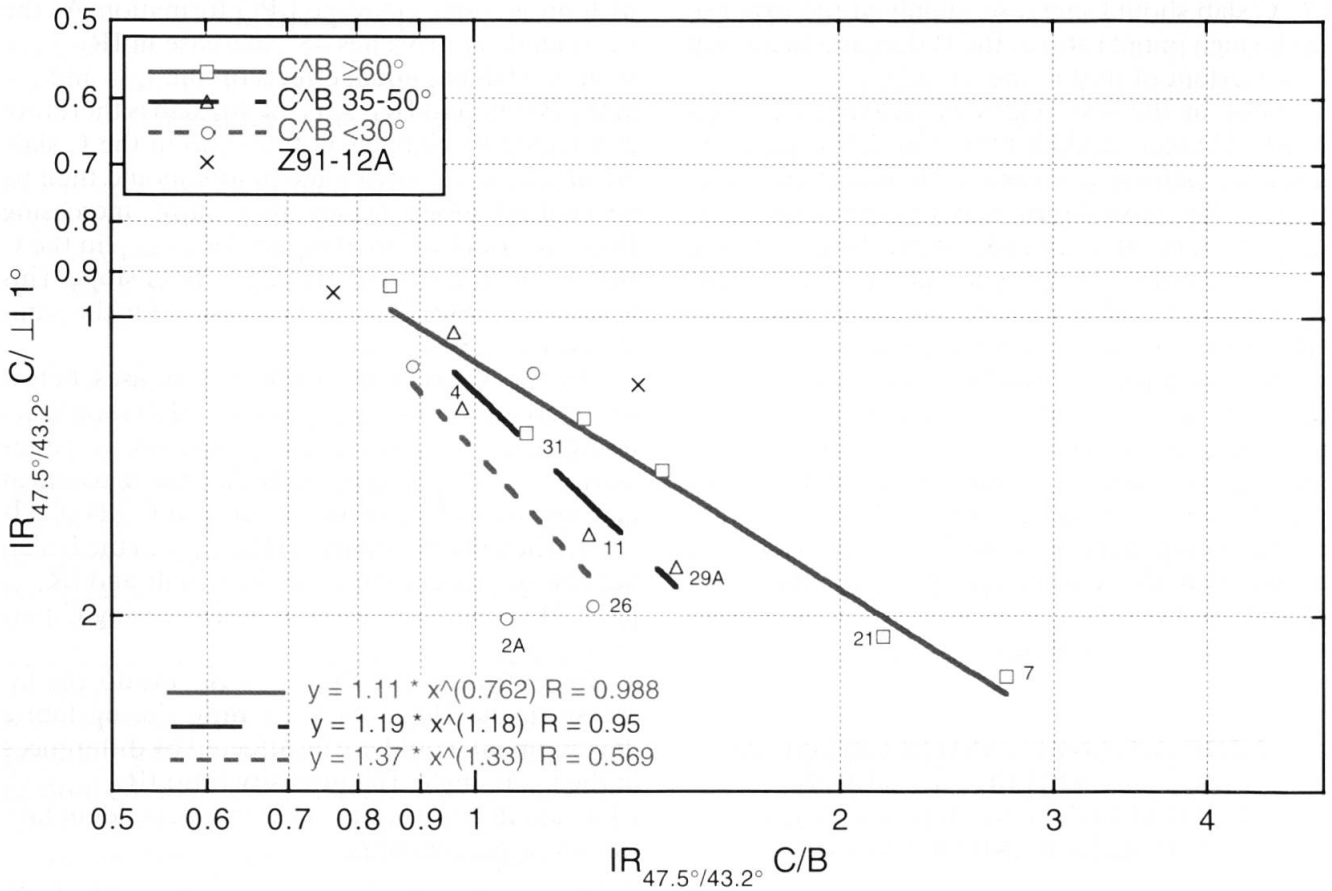

Fig. 7 Plot of $IR_{47.5°/43.2°}$ C/⊥I vs. $IR_{47.5°/43.2°}$ C/B. Most of the rocks plot on an approximately $IR_{47.5°/43.2°}$ B/⊥I-constant band. For rocks with identical initial bedding anisotropy, the value of $IR_{47.5°/43.2°}$ C/B at the intersection of the projected mean trend of their distribution with the $IR_{47.5°/43.2°}$ C/⊥I = 1 axis should constitute the $IR_{47.5°/43.2°}$ C_0/B_0 ratio of this lithology before deformation. The intensity ratio $IR_{47.5°/43.2°}$ C/⊥I would then be relatively independent of the initial anisotropy, and therefore constitute a more appropriate deformation index for a given deformation style. The sample Z91-12A, in which the calcite fabric is mainly due to coarse veins is not inclued in the regression.

stitutes a more appropriate deformation index for a given lithology and deformation style. Without going extensively into the details of method, we can apply an analogous method on the basis of intensity ratios of calcite reflections in the C , B and ⊥I slabs.

It can be shown that the length of the axis of the ellipsoid described by the fissility dimension in the direction normal to each of the sections is analogous to the reciprocal of $IR_{47.5°/43.2°}$ intensity ratio on that section, i.e.:

the *b* fissility-fragment dimension to the reciprocal of the $IR_{47.5°/43.2° C}$ intensity ratio;

the *c* fissility-fragment dimension to the reciprocal of the $IR_{47.5°/43.2° B}$ intensity ratio; and

the *i* fissility-fragment dimension to the reciprocal of the $IR_{47.5°/43.2° \perp I}$ intensity ratio.

Consequently, the X-ray-intensity-ratio analogues of the fissility-fragment dimension ratios of DURNEY and KISCH (1994) are :

the *c/b* fissility ratio: $(1{:}IR_{47.5°/43.2° B}) / (1{:}IR_{47.5°/43.2° C}) = IR_{47.5°/43.2° C} / IR_{47.5°/43.2° B}$ ($IR_{47.5°/43.2°}$ C/B).

the *i/c* fissility ratio: $(1{:}IR_{47.5°/43.2° \perp I}) / (1{:}IR_{47.5°/43.2° B}) = IR_{47.5°/43.2° B} / IR_{47.5°/43.2° \perp I}$ ($IR_{47.5°/43.2°}$ B/⊥I).

the *i/b* fissility ratio: $(1{:}IR_{47.5°/43.2° \perp I}) / (1{:}IR_{47.5°/43.2° C}) = IR_{47.5°/43.2° C} / IR_{47.5°/43.2° \perp I}$ ($IR_{47.5°/43.2°}$ C/⊥I).

Thus the $IR_{47.5°/43.2°}$ C/⊥I vs. $IR_{47.5°/43.2°}$ C/B plot introduced earlier is the equivalent of the *i/b* vs. *c/b* plot of DURNEY and KISCH (1994).

6.5. EFFECTS OF AN INITIAL BEDDING-PARALLEL FABRIC ON THE VARIATION OF THE $IR_{47.5°/43.2°}$ RATIOS UPON LPO DEVELOPMENT

In rocks with an initial, pre-deformational B-normal calcite *c*-axis fabric, the initial $IR_{47.5°/43.2°}$ C_0/B_0 at $IR_{47.5°/43.2°}$ $C_0/\perp I_0 = 1$ is below unity. Upon superimposition of a C-normal *c*-axis fabric upon such an initial fabric at a high angle to bedding, $IR_{47.5°/43.2°}$ will increase in the C slab, and decrease to the same extent in the B and the ⊥I-slab, so that on the $IR_{47.5°/43.2°}$ C/⊥I vs. $IR_{47.5°/43.2°}$ C/B plot the

$IR_{47.5°/43.2°}$ B/⊥I ratio remains constant, but at a higher value than for initially random fabrics. The value of $IR_{47.5°/43.2°}$ C/B at the intersection of the projected mean trend of these distributions with the $IR_{47.5°/43.2°}$ C/⊥I = 1 axis will then constitute the $IR_{47.5°/43.2°}$ C_0/B_0 ratio, a measure of the initial anisotropy of this lithology before deformation, in analogy to the initial c_0/b_0 ratio of DURNEY and KISCH (1994). The intensity ratio $IR_{47.5°/43.2°}$ C/⊥I will be relatively independent of the initial anisotropy.

At smaller C∠B angles, the decrease of $IR_{47.5°/43.2°}$ in the B slab upon development of a C-normal calcite fabric becomes progressively less than at C∠B = 90°, whereas in the ⊥I slab it remains similar to what it would be at C∠B = 90°. As a result, the $IR_{47.5°/43.2°}$ C/B and $IR_{47.5°/43.2°}$ C/⊥I ratios both plot at much higher values than at C∠B = 90°, whereas the B/⊥I ratio varies much less. In order to compare the position of points for smaller C∠B angles on the $IR_{47.5°/43.2°}$ C/⊥I vs. C/B plots with those of the same initial fabric but flattened at C∠B = 90°, they have therefore to be moved to appropriately lower values of $IR_{47.5°/43.2°}$ C/⊥I and C/B.

The measurements are shown on a $IR_{47.5°/43.2°}$ C/⊥I vs. $IR_{47.5°/43.2°}$ C/B plot is shown as Fig. 7. The regression through the points with C∠B ≥60° is very roughly at constant $IR_{47.5°/43.2°}$ B/⊥I, and the regressions through most of the points with ≤45° have a steeper $IR_{47.5°/43.2°}$ B/⊥I slopes, although there is no evidence that the rocks have a similar initial lithological anisotropy. Note that the samples for which increases in $I_{47.5°}$* and decreases in $I_{43.2°}$* in the C slabs are compensated by opposite changes in the ⊥I slabs, but apparently *not* (samples 2A, 4 and 26 – C∠B =25–45°), or only to a much lesser degree (e.g. 11, 29A, and 31 – C∠B =40–60°) in the B slabs plot below the regression for the points with C∠B ≥60°, possibly suggesting a lower value of $IR_{47.5°/43.2°}$ C_0/B_0, i.e. a stronger initial bedding anisotropy.

In accordance with the above-mentioned effect of small C∠B angles, the points for samples with small C∠B angles, notably Z91-2A and 26, have to be shifted to smaller values of $IR_{47.5°/43.2°}$ C/⊥I and $IR_{47.5°/43.2°}$ C/B for comparison with those of the same initial fabric but flattened at C∠B = 90°. The low B/⊥I values of these samples suggests the initial presence of a bedding parallel fabric. For the outlying point for sample Z91-2A, a strong B-parallel phyllosilicate fabric has been confirmed by SEM observation.

Absence of low $IR_{47.5°/43.2°}$ ratios in the B slabs might also be due to calcite crystals with their *c*-axes subnormal to I but subparallel to C, conceivably reflecting development of *c*-axis fibers due to extension in the X direction of the strain (DURNEY and RAMSAY, 1973).

6.6. A DEFORMATION INDEX OR INDEX FOR EXTENT OF TECTONIC FABRIC DEVELOPMENT

We have noted above that the intensity ratio $IR_{47.5°/43.2°}$ C/⊥I is relatively independent of both the angle C∠B and the initial anisotropy, and therefore may constitute a more appropriate deformation index or index for extent of tectonic fabric development for a given deformation style, in analogy to the intersection/bedding fissility index *i/b* of DURNEY and KISCH (1994, p. 271), which indicates the extent of tectonic fabric in rocks of different initial bedding anisotropy.

DURNEY and KISCH (1994, pp. 281–282) have warned that *i/b* is not totally independent of lithology – illustrating this by showing the difference in *i/b* in three distinct rock types in one outcrop, a mudstone and a tuffaceous sandstone (*i/b* = 1.5), and a siliceous argillite (*i/b* = 5). They conclude that "neither *c/b* or *i/b* may be assumed to be an universal indicator of deformation intensity in all rock types; the value of these measurements lies chiefly in their use for characterising deformation and fabric intensity in a single lithology". However, as the rocks discussed here constitute a rather restricted range of marly mudstone lithologies, use of the intensity ratio $IR_{47.5°/43.2°}$ C/⊥I as a deformation index or index for extent of tectonic fabric development for a given deformation style, independent of either the initial anisotropy or the C∠B angle, is attractive. Its use would suggest that samples Z91-7 and 21, and to a somewhat lesser extent Z91-2A, 11, 26, and 29A are among the most deformed rocks of the series studied., However, this use of *i/b* and the analogous $IR_{47.5°/43.2°}$ C/⊥I ratio have to be further investigated.

6.7. COMPARISON OF CALCITE AND PHYLLOSILICATE FABRICS

The rocks studied here show an appreciable anisotropy in phyllosilicate fabrics (KISCH, 1998). On Fig. 8, the calcite fabric parameter $IR_{47.5°/43.2°}$ C/B has been plotted against the relative cleavage/bedding mica fabric parameter $I_{10Å\ C}/I_{10\ Å\ B}$ ($I_{10Å}$ C/B). Note that strong mica fabrics are also detected only in the samples with large C∠B angles. The calcite fabric development is much less than that of the mica fabric: only when a strong cleavage-parallel mica fabric is developed is there an appreciable development of calcite fabric, and even then it is much weaker than the mica fabric. The persistence of a distinct bedding-parallel mica fabric in the microlithons of the crenulated

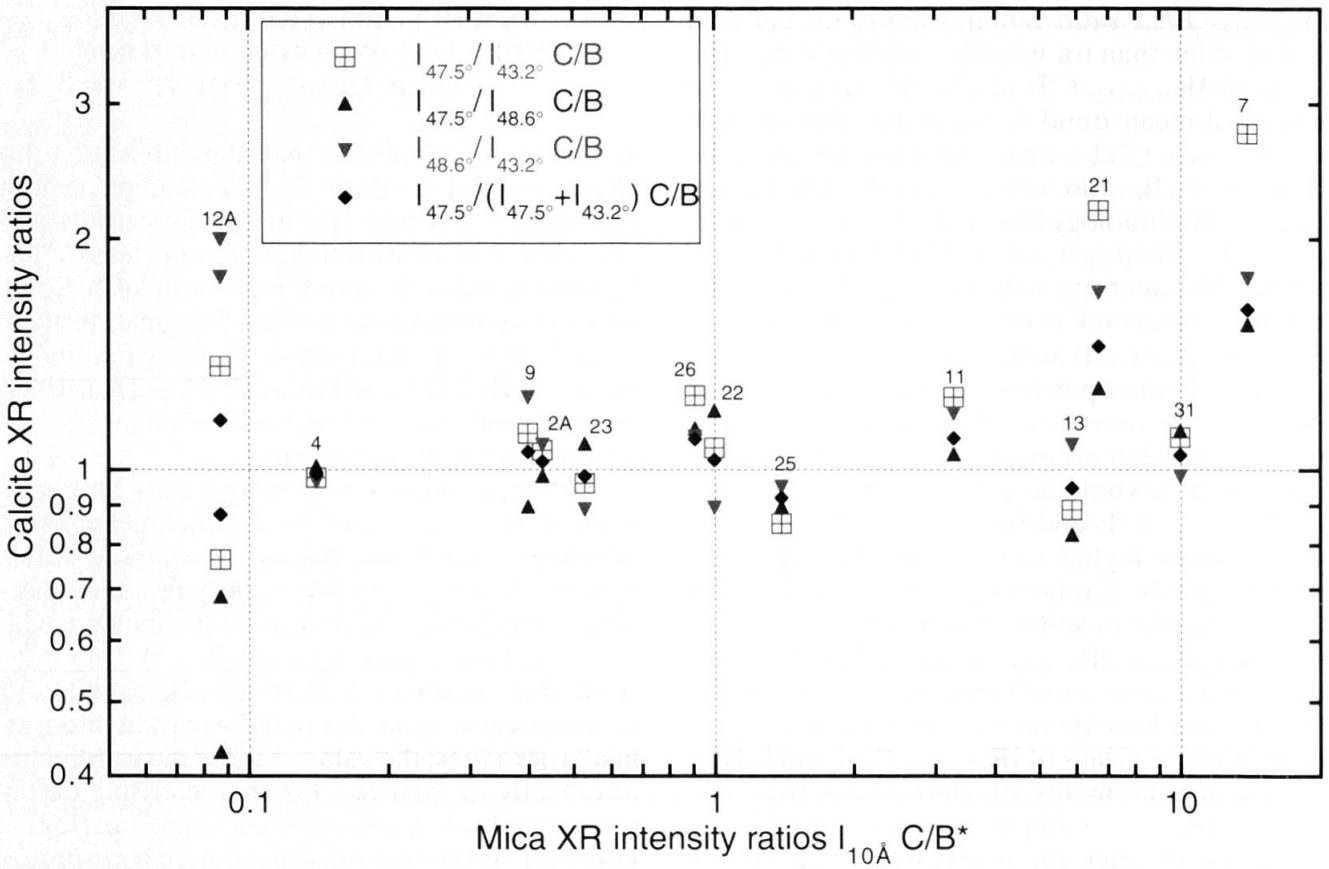

Fig. 8 Relationship of the of the calcite orientation-parameter ratios $IR_{47.5°/43.2°}$, $I_{47.5°}/I_{48.6°}$, $I_{48.6°}/I_{43.2°}$, and $I_{47.5°}/(I_{47.5°} + I_{43.2°})$ in the C slab to those in the B slab against the mica orientation parameter $I_{10\,Å}$ C/B (KISCH, 1998).

samples Z91-2A, 4 and 9, attested by $I_{10\,Å}$ C/B ratios well below unity, is not evident from the calcite C/B intensity ratios, but its former existence in sample Z91-2A, and to a much lesser extent in sample 4, appears to be indicated by their positions on the $IR_{47.5°/43.2°}$ C/⊥I vs. $IR_{47.5°/43.2°}$ C/B plot (see Fig. 7 and text). Considering that $IR_{47.5°/43.2°}$ is the ratio of two variables that vary in opposite directions upon cleavage formation, and therefore exaggerate the fabric effects, the contrast in intensity of the phyllosilicate and calcite fabrics is even more obvious, as becomes apparent if one of the parameters, i.e. either $I_{47.5°}$ or $I_{43.2°}$, is plotted against an approximate parameter of calcite content, such as $I_{48.6°}$ or $I_{47.5°} + I_{43.2°}$ (Fig. 8).

This discrepancy between phyllosilicate and calcite fabrics has implications for the respective orientation mechanisms of these minerals upon cleavage formation at very low grades of metamorphism. The relatively weak calcite reorientation appears to indicate a major contribution of pressure solution, and precludes wholesale phyllosilicate re-orientation due to matrix recrystallization: the phyllosilicate reorientation must largely be due to their passive mechanical reorientation into cleavage domains by removal of matrix by pressure solution, and subordinate recrystallization in the cleavage domains.

7. Conclusions

Comparison of the $IR_{47.5°/43.2°}$ intensity ratios of calcite measured on slabs parallel to bedding, cleavage, and normal to the bedding/cleavage intersection detects differences in calcite fabric and thus provide information on the development of a calcite LPO fabric during incipient cleavage development in low-grade metamorphic phyllosilicate-rich rocks. In particular it detects *c*-axis or $e\{01\bar{1}2\}$-pole LPO fabrics normal to bedding or cleavage, or partly transposed from bedding to cleavage. The most prevalent effect is the development of *c*-axis or *e*-pole fabric subnormal to the bedding/cleavage intersection I – with $IR_{47.5°/43.2°}$ ⊥I values largely ranging between 0.7 and 1.0 –, but variably oriented with respect to C and B. Prevalence of a B-subnormal *c*-axis or *e*-pole fabric is considered to represent a earlier bedding parallel slaty cleavage. The calcite shows a much weaker LPO fabric than the phyllosilicate.

The information obtained is approximate, but cannot be obtained by other simple methods in the presence of major mica-type clay minerals and albite.

Special account has to be taken of the effects of oblique angles between bedding and cleavage in reducing the difference between the intensity ratios in bedding- and cleavage-parallel slabs, and increasing the $IR_{47.5°/43.2°}$ B/⊥I ratios upon development of a *c*-axis fabric normal to C. Plots of $IR_{47.5°/43.2°}$ C/⊥I vs. $IR_{47.5°/43.2°}$ C/B can be used to establish the degree of tectonic calcite-fabric development in samples with different initial calcite *c*-axis fabrics. Admittedly, at small C∠B angles $IR_{47.5°/43.2°}$ in the C and B slab will mutually influence each other and converge, a high $IR_{47.5°/43.2°}$ B enhancing $IR_{47.5°/43.2°}$ in the C slab, but this will equally affect the $IR_{47.5°/43.2°}$ C/⊥I and $IR_{47.5°/43.2°}$ C/B ratios and different pre-deformational bedding-parallel fabric. The $IR_{47.5°/43.2°}$ C/⊥I ratio is tentatively adopted as an index for the intensity of tectonic calcite-fabric development.

Acknowledgments

The author acknowledges TGA analyses of carbonate content by Dr Gerd Jacob at the Martin-Luther Universität, Halle, Germany – untimely deceased in 2001 at the age of 39. The X-ray diffractometer was operated by Mrs Esther Shani and Mrs Dida Banai. Thanks to Drs Gerhard Oertel (Los Angeles) and Hans de Bresser (Utrecht), who read an earlier version of this paper and suggested improvements. Perspicacious comments by Prof. Martin Burkhard (Neuchâtel) and one anonymous referee led to major improvements in the paper. This paper ist dedicated to the memory of Bernard Kübler and Martin Frey, in recognition of their major contributions to the study of very low-grade metamorphism, and in gratitude for fruitful cooperation over a period of many years.

References

CASEY, M., RUTTER, E.H., SCHMID, S.M., SIDDANS, A.W.B. and WHALLEY, J.S. (1978): Texture development in experimentally deformed calcite rocks. In: GOTTSTEIN, G. and LÜCKE, K. (eds): Proc. 5th Int. Conf. Textures of Materials, Vol. 2. Springer, Berlin, 231–240.

DE BRESSER, J.H.P. (1989): Calcite c-axis textures along the Gavarnie thrust zone, central Pyrenees. Geol. Mijnbouw 68, 367–375.

DIETRICH, D. (1986): Calcite fabrics around folds as indicators of deformation history. J. Struct. Geol. 8 (6), 655–668.

DIETRICH, D. and SONG, H. (1984): Calcite fabrics in a natural shear environment, the Helvetic nappes of western Switzerland. J. Struct. Geol. 6 (1/2), 19–32.

DURNEY, D.W. and KISCH, H.J. (1994): A field classification and intensity scale for first-generation cleavages. AGSO Journal of Australian Geology and Geophysics 15 (3), 257–295.

DURNEY, D.W. and RAMSAY, J.G. (1973): Incremental strains measured by syntectonic crystal growth. In: DE JONG, K.A. and SCHOLTEN, R. (eds): Gravity and Tectonics. Wiley, New York, 67–96.

FRIEDMAN, M. and HIGGS, N.G. (1981): Calcite fabrics in experimental shear zones. In: CARTER, N.L., FRIEDMAN, M., LOGAN, J.M. and STEARNS, D.W. (eds): Mechanical Behaviour of Crustal Rocks: The Handin Volume. American Geophysical Union, Geophysical Monograph 24, 11–27.

KISCH, H.J. (1998): Criteria for incipient slaty and crenulation cleavage development in Tertiary flysch of the Helvetic zone of the Swiss Alps. J. Struct. Geol. 20 (5), 601–615.

LAFRANCE, B., WHITE, J.C. and WILLIAMS, P.F. (1994): Natural calcite c-axis fabrics: an alternate interpretation. Tectonophysics 229, 1–18.

PATERSON, S.R., YU, H. and OERTEL G. (1995): Primary and tectonic fabric intensities in mudrocks. Tectonophysics 247, 105–119.

RAMSAY, J.G. and HUBER, M.I. (1983): The Techniques of Modern Structural Geology. Volume 1: Strain Analysis. Academic Press, London, 307 pp.

RATSCHBACHER, L., WENK, H.R. and SINTUBIN, M. (1991): Calcite textures: examples from nappes with strain-path partitioning. J. Struct. Geol. 13, 369–384.

RUTTER, E.H. and RUSBRIDGE, M. (1977): The effect of non-coaxial strain paths on the crystallographic preferred orientation development in the experimental deformation of a marble. Tectonophysics 39, 73–86.

RUTTER, E.H., CASEY, M. and BURLINI, L. (1994): Preferred crystallographic orientation during the plastic and superplastic flow of calcite rocks. J. Struct. Geol. 16 (10), 1431–1446.

SCHMID, S.M., CASEY, M. and STARKEY, J. (1981): The microfabric of calcite tectonites from the Helvetic nappes (Swiss Alps). In: MCCLAY, K. and PRICE, N.J. (eds): Thrust and Nappe Tectonics . Spec. Publ. Geological Society of London 9, 151–158.

SCHMID, S.M., PANOZZO, R. and BAUER, S. (1987): Simple shear experimenrts on calcite rocks: rheology and microfabric. J. Struct. Geol. 9 (5/6), 747–778.

SINTUBIN, M. (1994): Phyllosilicate preferred orientation in relation to strain path determination in the lower Paleozoic Stavelot-Venn Massif (Ardennes, Belgium). Tectonophysics 237, 215–231.

TROMMSDORFF, V. (1964): Gefügestudien an Calcitmarmor aus Val Prato (Tessin). Schweiz. Mineral. Petrogr. Mitt. 44, 595–611.

WENK, H.-R. (1985): Carbonates. In: WENK, H.R. (ed.): Preferred Orientation in Deformed Metals and Rocks: an Introduction to Modern Texture Analysis. Academic Press, Orlando, 361–384.

WKENK, H.-R., TAKESHITA, T., BECHLER, E., ERSKINE, B.G. and MATTHIES, S. (1987): Pure shear and simple shear calcite textures. Comparison of experimental theoretical and natural data. J. Struct. Geol. 9, 731–745.

WENK, H.-R., VENKITSUBRAMANYAN, C.S. and BAKER, D. (1973): Preferred orientation in experimentally deformed limestone. Contrib. Mineral. Petrol. 38, 81–114.

Manuscript received September 20, 2001; revision accepted July 15, 2002.
Editorial handling: S.Th. Schmidt